The molecular landscape of pediatric acute myeloid leukemia reveals recurrent structural alterations and age-specific mutational interactions

Hamid Bolouri[1#*], Jason E Farrar[2#], Timothy Triche Jr[3#•], Rhonda E Ries[4#], Emilia L Lim[5]; Todd A Alonzo[6,7]; Yussanne Ma[5]; Richard Moore[5]; Andrew J Mungall[5]; Marco A Marra[5]; Jinghui Zhang[8]; Xiaotu Ma[8]; Yu Liu[8]; Yanling Liu[8]; Jaime M Guidry Auvil[9]; Tanja M Davidsen[9]; Patee Gesuwan[9]; Leandro C Hermida[9]; Bodour Salhia[10]; Stephen Capone[3]; Giridharan Ramsingh[3]; Christian Michel Zwaan[11]; Sanne Noort[11]; Stephen R Piccolo[12,13]; E Anders Kolb[14]; Alan S Gamis[15]; Malcolm A Smith[16]; Daniela S Gerhard[9]; and Soheil Meshinchi[4*]

[1]Division of Human Biology, Fred Hutchinson Cancer Research Center, Seattle, WA; [2]Winthrop P Rockefeller Cancer Institute, University of Arkansas for Medical Sciences and Arkansas Children's Research Institute, Little Rock, AR; [3]Jane Anne Nohl Division of Hematology, USC/Norris Comprehensive Cancer Center, Los Angeles, CA; [4]Clinical Research Division, Fred Hutchinson Cancer Research Center, Seattle, WA; [5]Canada's Michael Smith Genome Sciences Centre, British Columbia Cancer Agency, Vancouver, BC, Canada; [6]Keck School of Medicine, University of Southern California, Los Angeles, CA; [7]Children's Oncology Group, Monrovia, CA; [8]Division of Computational Biology, St Jude Children's Research Hospital, Memphis, TN; [9]Office of Cancer Genomics, National Cancer Institute, Bethesda, MD; [10]Department of Translational Genomics, Keck School of Medicine, University of Southern California, Los Angeles, CA; [11]Dept of Pediatric Oncology, Erasmus MC-Sophia Children's Hospital, Rotterdam, [12]Department of Biology, Brigham Young University, Provo, UT; [13]Department of Biomedical Informatics, University of Utah, Salt Lake City, UT; [14]Nemours Center for Cancer and Blood Disorders, Alfred I. DuPont Hospital for Children, Wilmington, DE; [15]Division of Hematology/Oncology/Bone Marrow Transplantation, Children's Mercy Hospitals and Clinics, Kansas City, MO; [16]Cancer Therapy Evaluation Program, National Cancer Institute, Bethesda, MD

# Equal contribution
* corresponding author

• Current address: Van Andel Research Institute
333 Bostwick Avenue NE
Grand Rapids, MI, 49503

Abstract

We present the molecular landscape of pediatric acute myeloid leukemia (AML), characterizing nearly 1,000 participants in Children's Oncology Group (COG) AML trials. The COG/NCI TARGET AML initiative assessed cases by whole-genome, targeted DNA, mRNA, miRNA sequencing and CpG methylation profiling. Validated DNA variants revealed diverse, infrequent mutations with fewer than 40 genes mutated in >2% of cases. In contrast, somatic structural variants, including novel gene fusions and focal *MBNL1*, *ZEB2*, and *ELF1* deletions, were disproportionately prevalent in young as compared to adult patients. Conversely, *DNMT3A* and *TP53* mutations, common in adults, are conspicuously absent from virtually all pediatric cases. Novel *GATA2*, *FLT3*, and *CBL* mutations, recurrent *MYC*-ITD, *NRAS*, *KRAS*, and *WT1* mutations are frequent in pediatric AML. Deletions, mutations, and promoter DNA hypermethylation convergently impact Wnt signaling, Polycomb repression, innate immune cell interactions, and a cluster of zinc finger genes associated with *KMT2A* rearrangements. These results highlight the need for, and facilitate the development of age-tailored targeted therapies for the treatment of pediatric AML.

Acute leukemia is the most common form of childhood cancer[1], and its incidence is increasing. Despite constituting only 20% of pediatric acute leukemia, acute myeloid leukemia (AML) is overtaking acute lymphoblastic leukemia (ALL) as the leading cause of childhood leukemic mortality, in part because current prognostic schemas classify many children who will ultimately succumb to their disease as low- or intermediate-risk. Additionally, aside from investigational tyrosine kinase inhibitors for *FLT3*-activated AML, targeted therapies are not used in pediatric AML. Both problems stem from an inadequate understanding of the biology of childhood AML.

AML is a molecularly heterogeneous group of diseases affecting patients of all ages[2]. Recent genome-scale studies have revealed novel, potentially targetable mutations prevalent in adult *de novo* AML[3-5]. However, the relevance of these findings to childhood AML remains unclear, since several of the most common adult mutations appear far less prevalent in pediatric AML[6,7].

To date, no comprehensive characterization of pediatric AML has been described. Here, we report the initial results of the TARGET (Therapeutically Applicable Research to Generate Effective Treatments) AML initiative, a collaborative COG/NCI project to comprehensively characterize the mutational, transcriptional, and epigenetic landscapes of a large, well-annotated cohort of pediatric AML. Comparing AML molecular profiles across age groups, we show that stark differences in mutations,d structural variants and DNA methylation distinguish AML in infants, children, adolescents, and adults.

Results

Overview of cohort characteristics

A total of 1023 children enrolled in COG studies are included in the TARGET AML dataset. Comprehensive clinical data, including clinical outcomes and test results for common sequence aberrations (outlined in **Table S1**), are available for 993 patients. Of these, 815 subjects were profiled for somatic mutations at presentation: 197 by whole-genome sequencing (WGS), and 800 by targeted capture sequencing (TCS), at read depths averaging 500x, for validation of mutations identified by WGS.

68 The WGS discovery cohort of diagnostic and remission (germline comparison) specimens were selected
69 from patients treated on recent COG studies who achieved an initial remission to induction
70 chemotherapy. These trials randomized type or timing of induction therapy (CCG-2961)[8] and the
71 addition of gemtuzumab ozogamicin in a single arm pilot (AAML03P1)[9] or randomized fashion
72 (AAML0531)[10]. Specimens for TCS validation were obtained from 800 patients, including 182 from the
73 WGS discovery cohort (153 with matched remission samples). A complete listing of cases and their
74 characterization is available in the TARGET sample matrix
75 (https://ocg.cancer.gov/programs/target/data-matrix). The age at presentation of TARGET AML
76 participants ranged from 8 days to 29 years (median 10 years, **Fig. 1a**). Infants (<3 years old), children
77 (age 3-14) and adolescents/young adults (AYA; age 15-39) differ broadly by cytogenetic and clinical risk-
78 group classifications (**Fig. 1a**, multivariate Chi-squared $p<10^{-22}$), consistent with observed differences in
79 clinically-evaluated structural abnormalities and mutations (summarized in **Fig. 1b**). Notably, among
80 these clinically detected abnormalities, only 5 mutations and 5 structural aberrations occur in more than
81 5% of patients (mutations in *FLT3*, *NPM1*, *WT1*, *CEBPA*, and *KIT*; fusions involving *RUNX1*, *CBFB* and
82 *KMT2A*; trisomy 8 and loss of the Y chromosome.)

83 We validated each class of somatic DNA sequence alteration discovered by WGS through secondary
84 assays (**Figs. 1c** and **S1**). Single nucleotide variants (SNVs) and short insertions and deletions (indels)
85 were confirmed by TCS of the coding sequences of the genes identified as recurrently altered in the
86 WGS studies. WGS-detected copy number alterations were confirmed by GISTIC2.0 scores from SNP
87 arrays; WGS-detected structural changes (such as translocations and inversions) were confirmed by
88 RNA-seq and clinical leukemia karyotyping data. Across variant types, we find >70% concordance
89 between at least two assays. These variants are referred to as verified variants hereon. An overview of
90 the multiplatform-verified somatic DNA variants in 684 patients is presented in **Fig. 2a**. Roughly a
91 quarter of patients possess normal karyotype, yet nearly all revealed at least one recurrent verified
92 somatic DNA alteration, and at least 12 common cancer-associated cellular processes are recurrently
93 impacted (**Fig. S2, Tables S2a, b**).

94 We carried out analyses of microRNA, mRNA, and/or DNA methylation in 412 subjects. A summary of
95 the assays performed and case-assay overlap is presented in **Fig. S3**. We compared our verified variants
96 to those of 177 adult AML cases from The Cancer Genome Atlas (TCGA) project[3], stratified by the age
97 groupings outlined in **Fig. 1a**. The TARGET and TCGA discovery cohorts both contained numerous AYA
98 patients (**Table S3**). Importantly, our conclusions regarding the molecular characteristics of this age
99 group are identical when analyzing either or both cohorts (**Fig. S4**).

100 **Somatic gene mutations in pediatric AML**

101 Like adult AML, pediatric AML has one of the lowest rates of mutation among molecularly well-
102 characterized cancers (**Fig. S5**), with < 1 somatic, protein-coding change per megabase in most cases.
103 However, the landscape of somatic variants in pediatric AML is markedly different from that reported in
104 adults[3,4] (**Figs. 2b, S6-S7, Table S4**). *RAS*, *KIT*, and *FLT3* alterations, including novel, pediatric-specific
105 *FLT3* mutations (FLT3.N), are more common in children. Mutational burden increases with age, yet older
106 patients have relatively fewer recurrent cytogenetic alterations. Indeed, the number of coding SNVs,
107 within and across cohorts, is best predicted by age (**Fig. 2c**, $p<10^{-15}$) and by cytogenetic subgroup. In
108 contradistinction to the higher prevalence of small sequence variants in older patients, recurrent
109 structural alterations, fusions, and focal copy number aberrations are more common in younger patients
110 (**Figs. 2d-e**, $p<10^{-3}$, see below). Patients with *CBFA2T3-GLIS2*, *KMT2A,* or *NUP98* fusions tend to have

111 fewer mutations ($p<10^{-9}$), with subgroups demonstrating inferior clinical outcome (**Fig. S8**). Patients with
112 core binding factor rearrangements tend to have more mutations than expected for their age ($p<10^{-15}$),
113 yet more favorable outcomes. The mutational spectrum of coding SNVs (**Fig. S5**) accumulates C→T
114 transitions with age ($p<10^{-3}$), with additional C→A transversions in t(8;21) ($p<10^{-2}$) and aberrant
115 karyotype ($p<10^{-2}$) patients.

116 After adjustment for cytogenetics and multiple comparisons, *NRAS* ($p<10^{-3}$) and *WT1* ($p<10^{-3}$) are
117 mutated significantly more often in younger patients, while *DNMT3A* ($p<10^{-23}$), *IDH1/2* ($p<10^{-4}$), *RUNX1*
118 ($p<10^{-4}$), *TP53* ($p<10^{-4}$), and *NPM1* ($p<0.03$) are mutated significantly more frequently in older patients.
119 *KRAS, CBL, GATA2, SETD2,* and *PTPN11* mutations appear to be more common in younger patients
120 ($0.05<p<0.1$, adjusted, **Figs. S7** and **S9**). We identified a prominent hotspot of *MYC* alterations[11] and
121 previously unreported internal tandem duplications appearing exclusively in children (**Fig. S7**). These
122 observations are replicated in an independent ECOG cohort (**Fig. S10a**) of 384 adult AML patients[5]. Since
123 gene fusions have characteristic cooperating mutations[12], we devised a weighted resampling scheme to
124 compare mutation frequencies in 584 TARGET and 131 TCGA AML cases while controlling for karyotypic
125 associations. The results (**Fig. S10b**) confirm the generality of the pediatric-adult differences identified
126 above.

127 For genes such as *CBL, GATA2, WT1, MYC* and *FLT3*, both the frequency and the sites of mutation often
128 differ between children and adults (**Figs. 3a** and **S7**), with multiple –frequently recurrent- alterations
129 distinct from those identified in adult AML. *RAS*-related mutations (mutant *KRAS*, *NRAS*, *PTPN11*, or *NF1*)
130 are common, particularly with *KMT2A* fusions (**Fig. S11, Tables S4-S6**). In addition to being more
131 common and varied, *WT1* mutations appear more likely to be of clonal origin in younger patients (**Fig.**
132 **3b**) despite the majority of pediatric patients presenting with multiple detectable sub-clones (**Fig. S12**).

133 These differences are clinically significant: we have previously shown that novel *FLT3* mutations are
134 functional, and yield poor responses to standard therapy[13]. The established adverse impact of *FLT3*-ITDs
135 on survival is significantly modulated by co-occurring variants, including *WT1* and *NPM1* mutations and
136 *NUP98* translocations. As shown in **Figs. 3c and S13-S14**, three independent, large-scale studies
137 demonstrate that *FLT3*-ITD accompanied by *NPM1* mutations is associated with relatively favorable
138 outcomes in pediatric patients, while *FLT3*-ITD with *WT1* mutations and/or *NUP98-NSD1* fusions yields
139 poorer outcomes than *FLT3*-ITD alone.

140 We found no coding mutations in *DNMT3A* in pediatric AML, despite its high frequency in adults.
141 Spontaneous deamination of 5-methylcytosine is strongly associated with aging, and *DNMT3A* contains
142 a CpG dinucleotide yielding hotspot R882 mutations by C-to-T deamination[14]. *DNMT3A* also directly
143 interacts with *TP53*[15], itself impacted far more frequently in adults. Mutations of *DNMT3A* or *TP53* drive
144 clonal hematopoiesis in many apparently healthy adults[16] but are rare in children, as are the *IDH1* and
145 *IDH2* mutations with which they often co-occur.

146 **The spectrum of somatic structural DNA changes in pediatric AML**

147 Many pediatric AML cases harbor chromosomal copy number changes distinct from those reported in
148 adults (**Fig. 4a**). Among the 197 cases assayed by WGS, we identified 14 novel focal deletions involving
149 *MBNL1*, a splicing regulator, or *ZEB2*, a key regulator of normal[17] and leukemic[18] hematopoiesis (**Fig.**
150 **S15**). Despite occurring on separate chromosomes, in regions devoid of other deletions, *MBNL1*:*ZEB2*
151 co-deletions occur far more often than expected ($p<10^{-13}$). Half of these accompany *KMT2A-MLLT3*

152 fusions (p=0.035, **Fig. S11, Tables S5-S6**). Samples with *MBNL1*:*ZEB2* co-deletions carry a larger number
153 of recurrent mutations (p=0.015), and *KMT2A*-fusion samples with del(MBNL1) or del(*ZEB2*) have a
154 larger number of additional cytogenetic abnormalities (p<0.0005). Another 15 novel, validated focal
155 deletions specifically impact *ELF1*, an ETS-family transcriptional regulator of *MEIS1*[19]. A statistically
156 significant difference in *ELF1* mRNA expression exists between *ELF1*-deleted and intact samples
157 (p<0.01), with 63 genes differentially expressed between the two groups (p<0.01, **Fig. S16**). Among
158 other novel recurrent copy losses, we note five heterozygous deletions of a region containing the *IL9R*
159 gene (**Table S5**) co-occurring with *KIT* mutations and t(8;21).

160 Consistent with our previous findings regarding *NUP98-NSD1* fusions[20], an expansive catalog of gene
161 fusions, many observed primarily or exclusively in pediatric cases, underscores the disproportionate
162 impact of structural variants in younger patients (**Figs. 4b** and **S17-S18**). But patterns of exclusion and
163 cooperation are not limited to patients with recurrent structural alteration*:* mutant *GATA2* is frequently
164 seen in children with normal karyotype (NK) AML, and both *GATA2* ($p<10^{-9}$) and *CSF3R* ($p<10^{-6}$, **Fig. S19**)
165 mutations co-occur with mutations of *CEBPA*[21]. *GATA2* and *CEBPA* are key regulators of
166 hematopoiesis[22,23], both interacting with *RUNX1* in normal hematopoiesis and leukemogenesis[24]. As with
167 *FLT3*/*NUP98-NSD1*/*WT1* interactions, these findings show prognostic interactions in pediatric AML
168 outcome (**Fig. S19b**). *RUNX1* mutations and *RUNX1-RUNX1T1* gene fusions are significantly exclusive of
169 *GATA2* and *CEBPA* mutations (p=0.006, **Fig. S20, Table S7**). All four are significantly exclusive of *KMT2A*
170 rearrangements ($p<10^{-15}$), *CBFB-MYH11* gene fusions ($p<10^{-11}$), and *ETV6* aberrations (p=0.01).

171 **DNA methylation subtypes in pediatric AML**

172 As summarized in **Fig. 4c**, aberrations affecting epigenetic regulators are widespread and rarely overlap
173 in AML, but their origin (structural vs. mutational) and frequency differs between children and adults.
174 Combining DNA methylation and mRNA expression results in 456 TARGET and TCGA AML cases, we
175 identified dozens of genes with recurrent transcriptional silencing via promoter hypermethylation across
176 TARGET and TCGA AML patients (**Figs. 5a and 5c, Tables S8-S9,** details in **Figs. S21-S22**). A number of
177 samples exhibited widespread silencing of genes by aberrant promoter hypermethylation, and this
178 group is enriched for younger patients with *WT1* mutations (p=0.0012, **Fig. 5a**, hyper-silenced group).
179 Aberrant Wnt/β-catenin signaling is required for the development of leukemic stem cells[25], and one or
180 more of the Wnt pathway regulators *DKK1*, *SMAD1, SMAD5, SFRP4, SFRP5, AXIN2, WIF1, FZD3, HES1,* or
181 *TLE1* is deleted or aberrantly methylated in most AML cases[26]. Repression of activating NK cell ligands
182 (particularly *ULBP1/2/3*) appears to be common in pediatric patients, which may represent a therapeutic
183 target[27]. In *KMT2A*-rearranged patients, a cluster of poorly characterized zinc finger genes on
184 chromosome 19 is recurrently silenced.

185 We applied non-negative matrix factorization (NMF) to CpG methylation data from 284 TARGET and
186 TCGA AML patients with DNA methylation data. By cross-validation, we identified 31 signatures (**Table**
187 **S10**) that best captured DNA methylation differences across samples, after controlling via *in silico*
188 purification for differences in cellularity. Unsupervised clustering of the resulting DNA methylation
189 signatures largely separated patients by age and karyotypic subtypes (**Figs. 5b and S23**), but also
190 revealed a signature which did not associate strongly with age or established prognostic factors
191 (Signature 13, **Fig. 5b**). Two signatures (signatures 2 and 13) predicted significantly ($p < 0.05$) poorer
192 event-free survival in both pediatric and adult patients with above-median scores, after stratifying by
193 cohort and adjusting for *TP53* mutation status and white blood cell count (**Fig. S24**). Larger sample sizes
194 are needed to evaluate the clinical significance of these findings.

195 **The pediatric AML transcriptome is shaped by diverse miRNAs**

196 We performed miRNA sequencing of 152 cases to characterize miRNA expression patterns in pediatric
197 AML. Unsupervised clustering of the data revealed 4 discrete subgroups that were correlated with
198 specific genomic alterations (**Figs. 6a** and **S25**), including high miR-10a expression in samples with *NPM1*
199 mutations, consistent with previous reports[28]. Further, Cox proportional hazards analyses identified
200 multiple miRNAs associated with clinical outcome (**Figs. S26-S28, Table S11**), including miR-155, which
201 we previously reported to predict poor survival[29].

202 Differential expression analyses using Wilcoxon tests revealed miRNAs that are differentially expressed
203 between pediatric and adult AML (**Fig. 6b**). Of note, miR-330 was the most over-expressed in pediatric
204 samples, and has previously been shown to have oncogenic potential in AML[30].

205 Several age-associated miRNAs harbor binding sites within, and have expression levels anti-correlated
206 with, putative target genes that may be involved in RNA and protein processing suggesting that miRNAs
207 could contribute to leukemogenesis through the dysregulation of transcripts and proteins[31]. Of note,
208 *let-7b,* which is a potential regulator of protein synthesis via *EIF2S3* (**Fig. 6c**), is typically less abundantly
209 expressed in pediatric AML (**Fig. 6d**). However, high *let-7b* expression in pediatric AML is associated with
210 shorter time to relapse (log-rank $p<0.05$, **Fig. 6e**).

211

212 Discussion

213 Using a large cohort of patients, this study establishes the prevalence of, and coincident relationships
214 among, recurrent somatic genetic and epigenetic abnormalities in pediatric AML. We observe several
215 features in common between pediatric and adult AML: a low overall mutation rate in comparison to
216 other cancers, a long tail of infrequently affected genes, and overlap among recurrently impacted genes.
217 However, pediatric AML exhibits distinctive and critically important characteristics. We and others have
218 previously reported on the presence and clinical impact of novel fusion genes in pediatric AML[20,32]. As
219 this study illustrates, the impact of fusion transcripts in AML is both broad and age-dependent.
220 Recognition and comprehensive testing for these alterations are key first steps in the development of
221 new and potentially novel modes of targeted therapy[33].

222 Recurrent focal deletions represent a unique aspect of pediatric AML. Regional (e.g. chromosomal arm-
223 and band-level) copy loss differs substantially by age, but surprisingly, focal areas of copy loss are also
224 more common in children, specifically impacting *ZEB2*, *MBNL1*, and *ELF1*. *MBNL1* is upregulated by the
225 *KMT2A-AF9* fusion protein[34], and genes involved in post-transcriptional processing (*SETD2, U2AF1,*
226 *DICER1*) harbor the sole recurrent mutation in several *KMT2A*-rearranged cases, suggesting a functional
227 role for altered splicing in pediatric leukemogenesis. Alterations in *ZEB2* have been identified as
228 cooperating events in murine *CALM-AF10* leukemia models[35] while *ZEB2* knockout mice develop
229 myelofibrosis[36], suggesting a fundamental role for this gene in the pathogenesis of AML.

230 Many of the genes characteristically mutated in AML are altered at widely variable frequencies across
231 age groups; several (including *FLT3* and *WT1*) are impacted by pediatric specific variants and hotspots.
232 Clinical tests for a handful of genomic alterations are widely used to risk-stratify patients and determine
233 treatment regimens. However, the current practice of considering the effect of each somatic alteration

234 in isolation is inadequate. As we illustrate for *FLT3*-ITD, interactions among sequence variants can have
235 dramatic clinical consequences. Moreover, some interactions appear to be age-specific. In pediatric
236 AML, *FLT3*-ITD and *NPM1* mutations co-occur in the absence of *DNMT3A* mutations in a group of
237 patients with superior outcomes (**Figs. 3c, S13 and S14**), in contrast to inferior outcomes reported in
238 adults where *FLT3*-ITD and *NPM1* mutations frequently co-occur with mutations in *DNMT3A*[4]. In the
239 TCGA adult AML cohort, over half the subjects with somatic *FLT3* and *NPM1* mutations also possessed
240 somatic *DNMT3A* mutations[3]. Subsequent studies established the generality of this result[4], and revealed
241 that *DNMT3A* mutations are early clonal events[37], which often co-operate with later *NPM1* and *FLT3*
242 mutations to promote chemoresistance, mutagenesis,[38] and inferior outcomes[39]. Similarly, the co-
243 occurrence of *FLT3*-ITD with *WT1* mutations or *NUP98-NSD1* fusions accompanies frequent induction
244 failure and dismal outcomes in children with AML (multivariate $p<10^{-4}$, **Figs. 3c, S13 and S14**).

245 In TARGET, TCGA, and ECOG AML cases, *WT1* mutations were mutually exclusive with those of *ASXL1*
246 and *EZH2* ($p < 10^{-3}$). *WT1* recruits *EZH2* to specific targets[40], and *WT1* mutations have been linked to
247 promoter DNA hypermethylation of *EZH2* target genes[41]. Mutant *ASXL1* abolishes *EZH2*-mediated
248 silencing of HOX genes[42]. *EZH2* resides on a recurrently deleted region of chromosome 7, and decreased
249 *EZH2* activity is associated with treatment resistant AML[43]. In pediatric AML, mutant *WT1* and *EZH2*
250 appear to be of exclusively clonal or near-clonal origin, with nearly a quarter of TARGET cases harboring
251 mutations affecting one or the other. Aberrant *WT1*, *EZH2*, or *ASXL1* predicted induction failure in
252 TARGET AML cases (multivariate $p<0.05$, adjusted for interactions with *FLT3* alterations*, NUP98-NSD1,*
253 and *KMT2A* fusions) and were largely mutually exclusive with *KMT2A* rearrangements ($p < 10^{-5}$). Many of
254 these patients present without apparent chromosomal abnormalities at diagnosis, yet less than 20%
255 achieve long-term remission with standard treatment, highlighting the importance of molecular
256 stratification to achieve better outcomes. It is possible that early events such as *WT1* mutations and
257 *NUP98-NSD1* fusions in children may play a similar role to that observed for *DNMT3A* mutations[14] in
258 adults, with significant implications for risk stratification in AML across age groups.

259 Our data also demonstrate that DNA-methylation and miRNA expression profiles both accompany and
260 complement DNA alterations, and can stratify pediatric AML patients in terms of both overall and
261 progression-free survival. These findings suggest a need to update pediatric AML clinical risk categories
262 beyond current classifications, with important implications for clinical practice.

263 Despite incremental improvements with increasingly intensified regimens, modern outcomes in
264 pediatric AML have plateaued, with only ~60% of patients achieving long term survival. As many as 10%
265 of children will die from direct complications of treatment. Survivors suffer unacceptably high rates of
266 long-term morbidities resulting from anthracycline exposure or sequelae of hematopoietic stem cell
267 transplantation. As illustrated herein, pediatric AML is a collection of molecularly diverse diseases with
268 similar phenotypes. No single treatment strategy is likely to be effective for all pediatric AML subtypes,
269 which may explain repeated failures of randomized clinical trials to improve outcomes in recent years. In
270 keeping with the shift towards comprehensive, molecularly based classification schemas in AML[4], the
271 time has come to develop targeted therapies that address specific vulnerabilities of pediatric subtypes.
272 The TARGET AML dataset will serve as a foundation for development of pediatric-specific classification
273 schemas and the development of personalized treatment strategies.

Acknowledgements

Dedicated to the memory of our colleague, mentor and friend, Dr. Robert Arceci, whose vision and perseverance set this effort in motion: “I may not have gone where I intended to go, but I think I have ended up where I needed to be.” (Douglas Adams, *The Long Dark Tea-Time of the Soul*)

The results published here are based upon data generated by the Therapeutically Applicable Research to Generate Effective Treatments (TARGET) initiative and The Cancer Genome Atlas. Data used for this analysis are available under dbGaP accession numbers phs000465 and phs000178. The TARGET initiative is supported by NCI Grant U10CA98543. Work performed under contracts from the National Cancer Institute, US National Institutes of Health within HHSN261200800001E includes specimen processing (the Children’s Oncology Group Biopathology Center), whole genomic sequencing (Complete Genomics) and RNA and targeted capture sequencing (British Columbia Cancer Agency). The content of this publication does not necessarily reflect the views or policies of the Department of Health and Human Services, nor does mention of trade names, commercial products, or organizations imply endorsement by the U.S. Government. Computation for the work described in this paper was supported in part by Fred Hutchinson Scientific Computing, the University of Southern California's Center for High-Performance Computing, and NSF award ACI-1341935. This work was additionally supported by COG Chairs U10CA180886 and U10CA98543; COG Statistics and Data Center U10CA098413 and U10CA180899; COG Specimen Banking U24CA114766; R01CA114563 (SM); St. Baldrick’s Foundation (JEF, TT, SM); Alex’s Lemonade Stand (SM), Target Pediatric AML (TpAML), P20GM121293 (JEF); Arkansas Biosciences Institute (JEF), and the Jane Anne Nohl Hematology Research Fund (TT).

Author Contributions

HB, JEF, TT and RER contributed equally to this work. MAS, DSG, SM and RA (see Acknowledgements) conceived and led the project. RER, MAM, JMGA, TMD, PG, LCH, DSG and SM managed the project. HB, JEF, TT, RER, ELL, TAA, YM, RM, AJM, MAM, JZ, XM, YuL, YaL, TMD, ACH, BS, and SRP generated, processed, and analyzed the data. SC, GR, CMZ, SN, EAK and ASG shared critical data and reagents. HB, JEF, TT, RER, ELL and SM drafted the manuscript. All authors edited and approved the manuscript.

Competing Financial Interests

The authors declare that they have no competing financial interests.

302 ## Figure Legends

303 **Figure 1. An overview of the TARGET AML study.** (**a**) The distribution of subjects by clinical risk category
304 and cytogenetic classification is shown adjacent to each age group analyzed (Infant, <3 years; Child, 3 to
305 <15 years; Adolescent/Young Adult (AYA), 15 to <40 years). (**b**) A summary of the clinically established
306 molecular aberrations in the cohort (n=993) is illustrated. FLT3.ITD, *FLT3* internal tandem duplications,
307 FLT3.PM, *FLT3* D835 point mutations. (**c**) Overview of the genomic variant discovery, verification, and
308 validation process. We characterized diagnostic and remission (taken as germline) samples from 197
309 patients using whole genome sequencing (WGS) and verified 153 diagnostic/remission case pairs by
310 targeted capture sequencing (TCS) of genes recurrently impacted in the WGS samples (an additional 29
311 WGS cases were verified by TCS of diagnostic cases only, see **Fig. S1**). 72% of WGS SNVs, and 76% of
312 WGS indels were confirmed by TCS (red & green text in figures). For focal copy number (CN) alterations
313 spanning fewer than 7 genes, 75% of recurrent WGS deletion/loss and 85% gain/amplification calls
314 matched recurrent alterations discovered by SNP6 arrays in 96 matching samples. For chromosomal
315 junctions, we integrated WGS, clinical karyotyping and RNA-seq data by majority vote, confirming 89%
316 of WGS junction calls.

317 **Figure 2. Age-related differences in mutational and structural alterations in AML. (a)** Distribution of
318 variants per sample. At least one variant impacting a gene recurrently altered in pediatric AML was
319 identified by multi-platform validated variants in 684 patients. Junction, protein fusions (see methods);
320 chromCNV, chromosomal arm/band level copy variant; focalCNV, gene level copy variant; indel, small
321 insertion/deletion; SNV, single nucleotide variant. (**b**) Age-dependent differences in the prevalence of
322 mutations. *FLT3* mutations are plotted in 3 categories: internal tandem duplication (ITD; FLT3.ITD),
323 activation loop domain (FLT3.C), and novel, childhood-specific changes (FLT3.N). (**b, inset**) A pattern of
324 waxing or waning mutation rates across age groups is evident in selected genes (*KRAS* and *NPM1*
325 illustrated). (**c**) Childhood AML, like adult AML, has a low somatic mutational burden (top and **Fig. S5**),
326 but is more frequently impacted by common cytogenetic alterations (lower section). For color key, see
327 legend at bottom-right. (**d**) The ratio of the burden of structural variation to SNVs/indels is high in
328 infancy and early childhood and declines with age. For color key, see legend at bottom-right. (**e**) Using a
329 sliding-window approach to account for uneven sampling by age, the incidence of common
330 translocations in AML is shown to follow age-specific patterns (multi-variate Chi-squared $p < 10^{-30}$), and
331 to be greatest in infants compared to all other ages (Chi-squared $p < 10^{-22}$). *KMT2A* fusions are most
332 common in infants (Chi-squared $p < 10^{-20}$), while core binding factor fusions tend to affect older children
333 (Chi-squared $p < 10^{-7}$).

334 **Figure 3. Biological and prognostic interactions between alterations of *WT1*, *NPM1*, *FLT3*-ITD and**
335 ***NUP98-NSD1*.** (**a**) *WT1* mutations appear more frequently and impact novel sites in childhood AML
336 (TARGET, expanded above the representation of *WT1*: 18.4%, 150 alterations among 815 patients;
337 TCGA, expanded beneath *WT1*: 7.3%, 13 alterations among 177 patients; Fisher's exact p = 0.0002).
338 Circles indicate sites of mutation with size proportional to the number of recurrently detected
339 alterations (Colors indicate type of mutation: red, frameshifting; blue, missense; yellow, nonsense;
340 purple, splice site; grey, in-frame deletions; and brown; in-frame insertions. (**b**) Inference of the clonal
341 origin of selected mutations in 197 TARGET AML (Infant, Child and AYA) cases with WGS and 177 TCGA
342 AML (Adult) cases. See Clonality Estimation section in the Online Methods for more details on how the
343 analysis was performed.. (**c**) The clinical impact of *FLT3*-ITD is modulated by other sequence aberrations.

963 TARGET patients had complete data for *FLT3*-ITD, *NPM1* and *WT1* mutation and *NUP98-NSD1* fusions. Patients with *FLT3*-ITD plus *WT1* and/or *NUP98-NSD1* fusion (n=73) exhibit markedly inferior event-free (multivariate p<0.001) and overall survival (see **Fig. S13**), while co-occurrence of *NPM1* mutations with *FLT3*-ITD associates with improved survival. These findings are confirmed by two separate studies from which TARGET cases were selected (AAML0531 and CCG-2961) as well as an independent cohort of patients treated on European cooperative group trials (DCOG, see online methods).

Figure 4. Chromosomal alterations in pediatric and adult AML patients. (**a**) Patterns of regional and chromosomal gain (outward projection) and loss (inward projection) in the TARGET (blue) and TCGA (red) AML cohorts. Losses of 5q, 7, and 17 predominate in adults, while gains of 4, 6, 19, and losses of 9, X, and Y are more common in younger patients. Chromosome numbers are printed on the outside and inside of the circle plot, and colored where there are large pediatric-adult differences. (**b**) Age-specific distributions of validated gene fusions. The fraction of events within an age group for each fusion pair is indicated by white-red shading, while the color of the fusion labels indicates the primary cytogenetic group (colors same as in **Fig. 1a**, see also **Figs. S17-S18**). The number in each box indicates the number of patients carrying the indicated translocation (labels at left). (**c**) Structural and mutational aberrations affecting epigenetic regulators in TARGET (WGS) and TCGA AML cohorts.

Figure 5. Aberrant DNA methylation in adult and pediatric AML. (**a**) Integrative analysis of genes with recurrent mutations, deletions, or transcriptional silencing by promoter DNA hypermethylation (rows) in TARGET and TCGA AML cases (columns). Cluster associations are labeled at the top, including a prominent group enriched for younger patients with *WT1* mutations (p=0.0012) that shows extensive transcriptional silencing across dozens of genes (blue boxed region, Hypersilenced). The cytogenetic group, *IDH1*/*2* mutation status (gray, mutated; white, wild-type or unknown) and TARGET/TCGA cohort membership for each sample is indicated below the main figure. The top marginal histogram indicates the total number of genes impacted for each patient. Gene/cytogenetic associations are shown to the right of the main figure, where per gene-rate of involvement by cytogenetic class is indicated by color and shading (unfilled = no involvement; full shading = maximum observed involvement of any gene within patients of the indicated cytogenetic grouping). Wnt regulators and activating NK cell ligands (e.g. *DKK1, WIF1* and *ULBP1, ULBP2, ULBP3,* respectively) are silenced across cytogenetic subtypes (labeled at far right). Distinct groups of silenced genes are also associated with *IDH1* or *IDH2* mutant patients and in *KMT2A*-rearranged patients. A subset of genes (56 of 119) altered in >3 patients and of patients (n=310; 168 TARGET, 142 TCGA subjects) with one or more genes silenced by promoter methylation is illustrated (see **Figs. S21-S22** and **Tables S8-S9** for enumeration of all 119 genes in all 456 evaluable subjects.). (**b**) A subset (16 of 31) of DNA methylation signatures derived by non-negative matrix factorization (NMF) and *in silico* purification, with samples ordered by hierarchical clustering of signatures (labeled at right). Genomic associations are indicated to the left of the main panel. Signature 13 does not correspond directly to known recurrent alterations, however, along with signature 2 displays potential prognostic significance (see **Fig. S24**). The patient-specific score matrix and display of all 31 signatures are provided in **Table S10** and **Fig. S23**. (**c**) Examples of expression/promoter DNA methylation relationships for *IL2RA* and *SFRP5*, 2 genes identified as recurrently silenced (panel **a**) which also contribute to NMF signatures (panel **b**) are shown. Y-axis: transformed expression (asinh(TPM)), x-axis: promoter CpG methylation. The vertical red line indicates the empirically established silencing threshold.

386 **Figure 6. miRNAs differentially regulate distinct molecular and age sub-groups in AML** (**a**)
387 Unsupervised clustering of miRNA expression patterns in 152 childhood AML cases identifies four
388 patient subgroups (colored bands at top) with correlation to somatic alterations as indicated (blue bars
389 on gray background), and subgroup-specific miRNA expression (miR-10 and miR-21 are highlighted as
390 examples). **(b)** Age-related differences in miRNA expression are evident between adult (n=162) and
391 pediatric AML (n=152). Volcano plot indicates differentially expressed miRNAs between adult and
392 pediatric cases. Red-green point shading indicates relative under- or over-expression in TARGET,
393 respectively. (Wilcoxon test, Benjamini-Hochberg adjusted $P<0.05$; Threshold indicated by dashed red
394 line). **(c)** A predicted miRNA:mRNA target relationship involving *let-7b*, which is (**d**) less abundant in
395 most pediatric cases than in adult cases. **(e)** High expression of *let-7b* occurs in a minority of pediatric
396 AML and is associated with shorter time to relapse.

397 ## References

398 1. Steliarova-Foucher, E.*, et al.* International incidence of childhood cancer, 2001-10: a population-
399 based registry study. *Lancet Oncol* **18**, 719-731 (2017).
400 2. Li, S.*, et al.* Distinct evolution and dynamics of epigenetic and genetic heterogeneity in acute
401 myeloid leukemia. *Nat Med* **22**, 792-799 (2016).
402 3. Cancer Genome Atlas Research, N. Genomic and epigenomic landscapes of adult de novo acute
403 myeloid leukemia. *N Engl J Med* **368**, 2059-2074 (2013).
404 4. Papaemmanuil, E.*, et al.* Genomic Classification and Prognosis in Acute Myeloid Leukemia. *N*
405 *Engl J Med* **374**, 2209-2221 (2016).
406 5. Patel, J.P.*, et al.* Prognostic relevance of integrated genetic profiling in acute myeloid leukemia.
407 *N Engl J Med* **366**, 1079-1089 (2012).
408 6. Ho, P.A.*, et al.* Leukemic mutations in the methylation-associated genes DNMT3A and IDH2 are
409 rare events in pediatric AML: a report from the Children's Oncology Group. *Pediatr Blood Cancer*
410 **57**, 204-209 (2011).
411 7. Farrar, J.E.*, et al.* Genomic Profiling of Pediatric Acute Myeloid Leukemia Reveals a Changing
412 Mutational Landscape from Disease Diagnosis to Relapse. *Cancer Res* **76**, 2197-2205 (2016).
413 8. Lange, B.J.*, et al.* Outcomes in CCG-2961, a children's oncology group phase 3 trial for untreated
414 pediatric acute myeloid leukemia: a report from the children's oncology group. *Blood* **111**, 1044-
415 1053 (2008).
416 9. Cooper, T.M.*, et al.* AAML03P1, a pilot study of the safety of gemtuzumab ozogamicin in
417 combination with chemotherapy for newly diagnosed childhood acute myeloid leukemia: a
418 report from the Children's Oncology Group. *Cancer* **118**, 761-769 (2012).
419 10. Gamis, A.S.*, et al.* Gemtuzumab ozogamicin in children and adolescents with de novo acute
420 myeloid leukemia improves event-free survival by reducing relapse risk: results from the
421 randomized phase III Children's Oncology Group trial AAML0531. *J Clin Oncol* **32**, 3021-3032
422 (2014).
423 11. Lavallee, V.P.*, et al.* Identification of MYC mutations in acute myeloid leukemias with NUP98-
424 NSD1 translocations. *Leukemia* **30**, 1621-1624 (2016).
425 12. Faber, Z.J.*, et al.* The genomic landscape of core-binding factor acute myeloid leukemias. *Nat*
426 *Genet* **48**, 1551-1556 (2016).
427 13. Tarlock, K.*, et al.* Discovery and Functional Validation of Novel Pediatric Specific FLT3 Activating
428 Mutations in Acute Myeloid Leukemia: Results from the COG/NCI Target Initiative. *Blood* **126**,
429 87-87 (2015).
430 14. Ley, T.J.*, et al.* DNMT3A mutations in acute myeloid leukemia. *N Engl J Med* **363**, 2424-2433
431 (2010).
432 15. Wang, Y.A.*, et al.* DNA methyltransferase-3a interacts with p53 and represses p53-mediated
433 gene expression. *Cancer Biol Ther* **4**, 1138-1143 (2005).
434 16. Genovese, G.*, et al.* Clonal hematopoiesis and blood-cancer risk inferred from blood DNA
435 sequence. *N Engl J Med* **371**, 2477-2487 (2014).
436 17. Goossens, S.*, et al.* The EMT regulator Zeb2/Sip1 is essential for murine embryonic
437 hematopoietic stem/progenitor cell differentiation and mobilization. *Blood* **117**, 5620-5630
438 (2011).
439 18. Goossens, S.*, et al.* ZEB2 drives immature T-cell lymphoblastic leukaemia development via
440 enhanced tumour-initiating potential and IL-7 receptor signalling. *Nat Commun* **6**, 5794 (2015).
441 19. Xiang, P.*, et al.* Identification of E74-like factor 1 (ELF1) as a transcriptional regulator of the Hox
442 cofactor MEIS1. *Exp Hematol* **38**, 798-798, 808 e791-792 (2010).

443 20. Ostronoff, F.*, et al.* NUP98/NSD1 and FLT3/ITD coexpression is more prevalent in younger AML
444 patients and leads to induction failure: a COG and SWOG report. *Blood* **124**, 2400-2407 (2014).
445 21. Maxson, J.E.*, et al.* CSF3R mutations have a high degree of overlap with CEBPA mutations in
446 pediatric AML. *Blood* **127**, 3094-3098 (2016).
447 22. Quintana-Bustamante, O.*, et al.* Overexpression of wild-type or mutants forms of CEBPA alter
448 normal human hematopoiesis. *Leukemia* **26**, 1537-1546 (2012).
449 23. Vicente, C., Conchillo, A., Garcia-Sanchez, M.A. & Odero, M.D. The role of the GATA2
450 transcription factor in normal and malignant hematopoiesis. *Crit Rev Oncol Hematol* **82**, 1-17
451 (2012).
452 24. Ng, K.P.*, et al.* Runx1 deficiency permits granulocyte lineage commitment but impairs
453 subsequent maturation. *Oncogenesis* **2**, e78 (2013).
454 25. Wang, Y.*, et al.* The Wnt/beta-catenin pathway is required for the development of leukemia
455 stem cells in AML. *Science* **327**, 1650-1653 (2010).
456 26. Valencia, A.*, et al.* Wnt signaling pathway is epigenetically regulated by methylation of Wnt
457 antagonists in acute myeloid leukemia. *Leukemia* **23**, 1658-1666 (2009).
458 27. Nanbakhsh, A.*, et al.* c-Myc regulates expression of NKG2D ligands ULBP1/2/3 in AML and
459 modulates their susceptibility to NK-mediated lysis. *Blood* **123**, 3585-3595 (2014).
460 28. Marcucci, G.*, et al.* MicroRNA expression in cytogenetically normal acute myeloid leukemia. *N*
461 *Engl J Med* **358**, 1919-1928 (2008).
462 29. Ramamurthy, R.*, et al.* miR-155 expression and correlation with clinical outcome in pediatric
463 AML: A report from Children's Oncology Group. *Pediatr Blood Cancer* **63**, 2096-2103 (2016).
464 30. Fooladinezhad, H., Khanahmad, H., Ganjalikhani-Hakemi, M. & Doosti, A. Negative regulation of
465 TIM-3 expression in AML cell line (HL-60) using miR-330-5p. *Br J Biomed Sci* **73**, 129-133 (2016).
466 31. Lim, E.L.*, et al.* Comprehensive Sequence Analysis of Relapse and Refractory Pediatric Acute
467 Myeloid Leukemia Identifies miRNA and mRNA Transcripts Associated with Treatment
468 Resistance - a Report from the COG/NCI-Target AML Initiative. *Blood* **126**, 687-687 (2015).
469 32. Gruber, T.A.*, et al.* An Inv(16)(p13.3q24.3)-encoded CBFA2T3-GLIS2 fusion protein defines an
470 aggressive subtype of pediatric acute megakaryoblastic leukemia. *Cancer Cell* **22**, 683-697
471 (2012).
472 33. Liang, K.*, et al.* Therapeutic Targeting of MLL Degradation Pathways in MLL-Rearranged
473 Leukemia. *Cell* **168**, 59-72 e13 (2017).
474 34. Itskovich SS, C.J., Mulloy JC, Disney MD, Kumar AR. MBNL1 As a New Therapeutic Target in MLL-
475 Fusion Gene Leukemia. in *Americal Society of Hematology Annual Conference* 462 (Orlando, Fl.,
476 2015).
477 35. Caudell, D.*, et al.* Retroviral insertional mutagenesis identifies Zeb2 activation as a novel
478 leukemogenic collaborating event in CALM-AF10 transgenic mice. *Blood* **115**, 1194-1203 (2010).
479 36. Li, J.*, et al.* The EMT transcription factor Zeb2 controls adult murine hematopoietic
480 differentiation by regulating cytokine signaling. *Blood* **129**, 460-472 (2017).
481 37. Shlush, L.I.*, et al.* Identification of pre-leukaemic haematopoietic stem cells in acute leukaemia.
482 *Nature* **506**, 328-333 (2014).
483 38. Guryanova, O.A.*, et al.* DNMT3A mutations promote anthracycline resistance in acute myeloid
484 leukemia via impaired nucleosome remodeling. *Nat Med* **22**, 1488-1495 (2016).
485 39. Loghavi, S.*, et al.* Clinical features of de novo acute myeloid leukemia with concurrent DNMT3A,
486 FLT3 and NPM1 mutations. *J Hematol Oncol* **7**, 74 (2014).
487 40. Xu, B.*, et al.* Tumor suppressor menin represses paired box gene 2 expression via Wilms tumor
488 suppressor protein-polycomb group complex. *J Biol Chem* **286**, 13937-13944 (2011).
489 41. Sinha, S.*, et al.* Mutant WT1 is associated with DNA hypermethylation of PRC2 targets in AML
490 and responds to EZH2 inhibition. *Blood* **125**, 316-326 (2015).

491 42. Abdel-Wahab, O.*, et al.* ASXL1 mutations promote myeloid transformation through loss of PRC2-
492 mediated gene repression. *Cancer Cell* **22**, 180-193 (2012).
493 43. Gollner, S.*, et al.* Loss of the histone methyltransferase EZH2 induces resistance to multiple
494 drugs in acute myeloid leukemia. *Nat Med* **23**, 69-78 (2017).
495

496

497 **Online Methods**

498 **Sample Selection and Preparation.** All patient samples were obtained by member COG institutions
499 after written consent from the parents/guardians of minors upon enrolling in the trial. The study was
500 overseen by the Institutional Review Board at Fred Hutchinson Cancer Research Center (Protocol 1642,
501 IR File #5236). Selected clinical (e.g., age, presenting hematological indices, cytogenetic classification)
502 and molecular features (e.g., *KIT*, *RAS*, *NPM*, *WT1*, *CEBPA*, *IDH1* mutations, and *FLT3*/ITD allelic ratios)
503 were clinically available prior to genomic analyses and are included in the clinical data file available at
504 the TARGET data matrix. 177 cases from the adult de novo AML TCGA dataset[3] were selected for
505 analysis after exclusion of those with FAB M3 morphology (n=20) or *BCR-ABL1* gene fusion (n=3) since
506 these subtypes are not represented in the COG/TARGET-AML cohort. The age distributions for the
507 TARGET WGS discovery group and the TCGA cohort are outlined in **Table S3**.

508 DNA and RNA was extracted from ficoll-enriched, viably cryopreserved samples from the COG
509 biorepository using the AllPrep Extraction Kit (Qiagen). Nucleic acids were quantified by NanoDrop
510 (Thermo Scientific). RNA samples were tested for quality and integrity using the Agilent 2100
511 Bioanalyzer (Agilent Technologies). The integrity of DNA samples was confirmed by visualization on a
512 0.8% agarose gel.

513 **Whole genome sequencing.** Sequencing libraries were constructed for WGS cases from genomic DNA
514 and sequenced using combinatorial probe anchor ligation by Complete Genomics (CGI)[44]. Reads were
515 mapped to the GRCh37 reference human genome assembly by the CGI Cancer Sequencing service using
516 software version 2.1 of the CGI cancer analysis pipeline (http://www.completegenomics.com/customer-
517 support/documentation/).

518 Somatic coding SNVs and indels were extracted from MAF files and filtered to remove 1) germline
519 variants; 2) low-confidence variants and 3) paralogs. For step 1, germline variants used for filtering
520 include those from NLHBI Exome Sequencing Project (http://evs.gs.washington.edu/EVS/), dbSNP 132
521 (https://www.ncbi.nlm.nih.gov/projects/SNP/), St Jude/Washington University Pediatric Cancer Genome
522 Project (PCGP), and CGI WGS from the TARGET project. For step 2, a mutation is considered of low-
523 confidence if it does NOT meet one of the following criteria: a) mutant allele has ≥3 more read count in
524 tumor than in the normal sample; b) the mutant read count in tumor is significantly higher than that in
525 the matched normal ($P<0.01$ by Fisher exact test); and c) mutant allele fraction in normal is below 0.05.
526 For step 3, we ran BLAT search using a template sequence that includes the mutant allele and its 20-bp
527 flanking region to determining the uniqueness of mapping of the mutation. To avoid over-filtering, we
528 implemented a rescue pipeline which retains all "gold" variants that match known somatic mutation
529 hotspots based on our variant classification program Medal Ceremony[45].

530 In addition to small variant calls (SNV, indel), the CGI cancer analysis pipeline delivered flat files of
531 potential novel DNA junctions and segmented copy number ratios derived from normalized read counts
532 from paired tumor/normal specimens. Circos summary plots of the unfiltered CGI data are available
533 through the data matrix. To reduce potentially spurious calls, final CNVs for analysis were trimmed after
534 empirical tuning to previously available Affymetrix SNP6 microarray calls in matched samples by
535 requiring a CGI average normalized coverage (avgNormCvg) in the region of ≥20 for putative non-
536 homozygous deletions, the SD for lesser allele fraction ≤ 0.22, a CGI ploidyScore of <30 and trimming of
537 calls on ChrM, centromeric or telomeric regions, and merged for adjacent CNV, per called direction,
538 within 10 Kbp. With these filters, 75 and 85% (loss and gain, respectively) of filtered CNV calls matched

539 CNVs previously called by Affymetrix SNP6 microarray and 87% of chromosome-arm level calls matched
540 reported karyotype abnormalities reported in the clinical data. Putative copy variants underwent further
541 secondary confirmation using the nanoString nCounter assay (Nanostring Technologies). Novel DNA
542 junctions discovered by WGS were included in cases where at least one additional level of support was
543 available, either from cytogenetic analysis or from RNA sequencing studies.

544 **Targeted Capture Sequencing.** Candidate genes identified by WGS analysis were selected for
545 independent verification in 182 samples from the WGS discovery cohort and 618 additional subjects
546 treated on COG AAML0531. Capture baits were designed and ordered using Agilent's SureDesign
547 (https://earray.chem.agilent.com/suredesign/) for these selected genes along with target regions
548 identified in concurrent TARGET studies, targeting coding regions and UTRs with a 10 bp pad. This design
549 (TARGET AML + TARGET other) resulted in an overall target space of 2.376 Mbp with 98.7% of target
550 regions covered by a probe. Probe density was specified at 2x, with moderately stringent repeat
551 masking, and balanced boosting options selected.

552 Genomic DNA libraries from which gene regions of interest are captured were constructed according to
553 British Columbia Cancer Agency Genome Sciences Centre (BCGSC) plate-based and paired-end library
554 protocols on a Biomek FX liquid handling robot (Beckman-Coulter, USA). Briefly, 1µg of high molecular
555 weight genomic DNA was sonicated (Covaris E210) in a 60µL volume to 200-300bp. Sonicated DNA was
556 purified with magnetic beads (Agencourt, Ampure). The DNA fragments were end-repaired,
557 phosphorylated and bead purified in preparation for A-tailing. Illumina sequencing adapters were
558 ligated overnight at 20°C and adapter ligated products bead purified and enriched with 4 cycles of PCR
559 using primers containing a hexamer index that enables library pooling. 94ng from each of 19 to 24
560 different libraries were pooled prior to custom capture using Agilent SureSelect XT Custom 0.5-2.9Mb
561 probes. The pooled libraries were hybridized to the RNA probes at 65°C for 24 hours. Following
562 hybridization, streptavidin-coated magnetic beads (Dynal, MyOne) were used for custom capture. Post-
563 capture material was purified on MinElute columns (Qiagen) followed by post-capture enrichment with
564 10 cycles of PCR using primers that maintain the library-specific indices. Paired-end 100 base reads were
565 sequenced per pool in a single lane of an Illumina HiSeq2500 instrument. Illumina paired-end
566 sequencing reads were aligned to the GRCh37-lite reference using BWA version 0.5.7. This reference
567 contains chromosomes 1-22, X, Y, MT, 20 unlocalized scaffolds and 39 unplaced scaffolds. Multiple lanes
568 of sequences were merged and duplicated reads were marked with Picard Tools. Small variants (SNV
569 and indel) from TCS data were identified by parallel methods, integrated, and subsequently filtered as
570 follows. **Mpileup**: SNVs were analyzed with SAMtools mpileup v.0.1.17 on paired libraries[46]. Each
571 chromosome was analyzed separately using the -C50-DSBuf parameters. The resulting vcf files were
572 merged and filtered to remove low quality variants by using samtools varFilter (with default parameters)
573 as well as to remove variants with a QUAL score of less than 20 (vcf column 6). Finally, variants were
574 annotated with gene annotations from ensembl v66 using snpEff[47] and the dbSNP v137 db membership
575 assigned using snpSift[48]. **Strelka**: Samples were analyzed pair wise with the default settings of Strelka[49]
576 v0.4.7 with primary tumor samples against the matched remission sample. Somatic variants called by
577 either Mpileup or Strelka were combined and filtered by meeting any of the following criteria: <10 reads
578 in the remission sample, <10 reads in the tumor sample, tumor alt base = 0, adjusted tumor allele
579 frequency = 0, gmaf >0.009, or >60 patients had exact SNV. For patients established to be in
580 morphological remission, additional filters included removing variants with >0.10 allele fraction in the
581 remission sample and a FET score of >0.05. For refractory patients, variants were excluded with >0.35

582 allele fraction in the post-Diagnostic sample. These filtered variants could be "rescued" if a variant was a
583 known COSMIC mutation associated with hematological cancers. The filtering criteria for indel calls
584 were similar. Tandem duplications were identified with Pindel using default parameters[50]. In addition,
585 clinical molecular testing for specific genes (*FLT3* ITD and *FLT3* codons 835/836, *CEBPA* bzip and NTD
586 regions, *KIT* exons 8 and 17, *CBL* exons 8 and 9, and *WT1* exon 7) were merged into the variant calls for
587 final analysis.

588 DNA variants from discovery and TCS studies were merged to construct the mutation profile for each
589 gene using the web-based program, ProteinPaint[51]. Genome-wide mutational burden was compared to
590 published data from, and using the method of, Lawrence et al[52].

591 ***CBL* Transcript Variant Screening by cDNA PCR.** Total RNA isolated from patient leukemic cells using the
592 Qiagen AllPrep DNA/RNA Mini Kit (Qiagen, Germany) was reverse transcribed to cDNA with oligo DT
593 primer and additional reagents following the Maxima H Minus First Strand cDNA Synthesis Kit
594 instructions (Thermo Scientific, Grand Island, NY).

595 Synthesis of the second-strand cDNA and following PCR were performed using the following primers:
596 forward primer for genemap: (5'FAM-TTCCAAGCACTGATTGATGG), forward primer for sequencing (5'-
597 TTCCAAGCACTGATTGATGG-3'), reverse primer: (5'-AACAGAATATGGCCGGTCTG). PCR was performed in
598 25uL volumes containing 12.5uL Failsafe Epicentre Buffer C (2x) (Epicentre Technologies, Madison, WI),
599 0.5uL (10uM) of each primer, 0.25uL Invitrogen Platinum Taq Polymerase (Thermo Scientific - Invitrogen,
600 Grand Island, NY), 1uL of cDNA, and 10.25uL of Nuclease-Free Water (USB Corporation, Cleveland, OH).
601 The Thermocycling program consisted of 5 min denaturation at 95 C, followed by 35 cycles at 95 C for 30
602 sec, 60°C for 30 sec and 72 C for 45 sec min and a final extension of 7 min at 72 C in a 96 well Biometra T
603 professional Thermocycler (Biometra, Germany)

604 PCR products were diluted in nuclease free water (USB Corporation, Cleveland, OH) and mixed with
605 deionized Formamide and GENESCAN-400HD (ROX) size markers (Applied Biosystems, Foster City, CA)
606 and submitted for electrophoresis on an ABI 3730 Genetic Analyzer (Applied Biosystems). After
607 electrophoresis the fluorescence signals were analyzed using GeneMapper 5.0 software (Applied
608 Biosystems). Genemapper screening revealed products of the expected WT normal size (685bp), and
609 additional products of various sizes: corresponding to complete deletion of Exon 8 (563bp), complete
610 deletion of Exon 9 (485bp), as well as deletion involving both CBL exon 8 and exon 9 (354bp).

611 Patients exhibiting deletions by Genemapper were then sent for sequence verification. PCR products
612 were treated with Exo-SAPit enzyme (USB Corporation, Cleveland, OH). Sequencing was done by
613 Eurofins MWG Operon LLC (Huntsville, AL) in accordance with their DNA sequencing process guidelines
614 and methods.

615 **Generalized linear mixed model for coding mutation counts.** In order to account for both fixed and
616 random effects which might be present with age and cytogenetic subgroups, we employed a generalized
617 linear mixed model (glmm, Knudson 2016, R package version 1.1.1, https://CRAN.R-
618 project.org/package=glmm) to model the discrete counts of coding SNVs in each TARGET and TCGA WGS
619 patient with a Poisson error distribution (log link). Marginal likelihood ratio tests for age (as a continuous
620 predictor) and cytogenetic subgroup (as a categorical predictor) were uniformly and highly significant, as
621 reported in the text, while the per-cytogenetic-group random effects accounted for a small (< 0.003%)
622 fraction of the variance observed. The model converged in 208 steps; 10,000 MCMC iterations were

623 employed to estimate the mixed effects component of the model, fitted per-cytogenetic-group
624 assuming a random slopes model.

625 **Generalized Dirichlet-multinomial regression for mutational spectra.** To accommodate the possibility
626 of either negative or positive correlation between the counts of each type of mutation (C→T, C→A,
627 C→G, T→C, T→A, T→G) in each subject, we employed a generalized Dirichlet-multinomial model
628 (mglm[53], R package version 0.0.7, https://CRAN.R-project.org/package=MGLM) with age and
629 cytogenetic group as predictors, mutational spectrum (a matrix of counts for each type of mutation) as
630 response. At convergence, the significant predictors of mutational spectrum differences were age (most
631 significant), t(8;21) status, and aberrant karyotype (mutually exclusive with t(8;21) and other common
632 recurrent chromosomal abnormalities). C→T transitions are known to increase with age, particularly for
633 methylated cytosines; however, an inflation of C→A transversions was particularly apparent in t(8;21)
634 and aberrant karyotype cases. (Both t(8;21) and inv(16) affect core binding factor subunits, and both are
635 associated with higher mutational burdens at a given age, but only t(8;21) cases show additional C→A
636 transversions beyond those expected from counts).

637 **Weighted resampling scheme to compare TARGET and TCGA mutation frequencies.** Common
638 chromosomal aberrations often co-occur with specific types of additional DNA sequence abnormalities.
639 To account for this observation when determining differences in mutation frequencies between TARGET
640 AML and TCGA AML, we first divided each cohort into the following categories: *KMT2A* fusions, t(8;21),
641 inv(16), del(7), +8, +21, -Y, and normal karyotype (NK). A total of 131 unique TCGA and 548 TARGET
642 samples fell into one of the above categories. We then sampled equal numbers of specimens from each
643 category and calculated the fraction of samples with mutations in a given gene. To account for sampling
644 variations, we repeated our sampling procedure 5000 times and calculated the mean and standard
645 deviation of the fraction of samples with mutations in each gene of interest.

646 **Variant pairwise mutual exclusion and co-occurrence.** Pairwise mutually exclusive sequence alterations
647 (**Fig S20a**) were identified using CoMEt[54] with the "exhaustive" option
648 (http://compbio.cs.brown.edu/projects/comet/). Pairwise co-occurrence p-values (Fig S20b) were
649 calculated directly using a hypergeometric distribution (equivalent to Fisher's exact test). Statistically
650 significant exclusion/co-occurrence patterns were visualized using Cytoscape[55] (http://cytoscape.org/),
651 with edge thickness representing –log10(p-value).

652 **Orthogonal evaluation of mutual exclusion and co-occurrence via penalized Ising model.** A slightly
653 different approach to reconstructing a binary-valued undirected graph (a discrete Markov random field)
654 employs penalized logistic regression of all candidate nodes upon each possible target and selects the
655 most probable graph structure based on extensions of the Bayes information criterion (EBIC). This
656 approach is implemented by Epskamp (https://cran.r-project.org/package=IsingFit)[56] and employs a
657 hyperparameter (γ) for the penalty weight which eventually determines the density of the estimated
658 network. Adjustment for multiple comparisons was applied to the marginal significance of each gene-
659 gene Fisher exact test; this value is not unbiased due to post-selection inference and is only intended as
660 a guide. The resulting network of correlated and anticorrelated binary indicators (gene- and
661 chromosomal-level aberrant/wildtype, pediatric/adult) recovers known and CoMEt-detected
662 relationships, but also identifies several novel and marginally significant (by Fisher's exact test, see
663 above) relationships, as summarized in Supplementary Table 6.

664 **Hypothesis-testing.** Except where described by the methods above, p-values are calculated by Fisher's
665 exact test; where an exact binomial test is impractical, we approximate this with a Chi-squared p-value.

666 **Regression fits for structural/sequence variant burden and age-associated recurrent abnormalities.** To
667 fit the ratio of structural to sequence variant impact in each patient, we added 0.333 as a smoothing
668 factor to the counts of each clonal event of each type, using all recurrently mutated, fused, or silenced
669 genes, identified in either cohort, as candidates for "impact" by structural variants. The transparency of
670 each data point represents its observed over expected mutational burden, given the patient's age, but
671 has no impact on the loess regression fit. The loess curve was fit by ggplot2 (http://ggplot2.org) on a
672 log10 scale. To estimate the relative contribution of each of the recurrent fusion neighborhoods across
673 ages (rather than age groups), we used the "zoo" time series package[57] to fit a rolling median with
674 expanding time steps (1, 3, 5, 8, 17) across all subjects for whom we had data on fusions. The
675 (smoothed) contribution of each family of fusions to the total number of patients in a given age window
676 (expanding with advancing age) is plotted in Figure 2d.
677
678 **Clonality estimation.** Several packages (including MAFtools[58] (https://github.com/PoisonAlien/maftools)
679 Gaussian mixture, SciClone's[59] beta mixture model, and a weighted penalized logistic mixture model)
680 were compared to validate the results obtained, in addition to manual review of all results. While
681 proportions of mutations assigned to various clones differed in some cases (especially with and without
682 read support weighting), the primary mutational clones were consistently identified by all methods, and
683 an overall tendency for childhood and AYA patients to present with greater diagnostic mutational
684 clonality, at the read depths available in the TARGET WGS and TCGA data, was confirmed by all
685 methods. Among AYA patients (where both TCGA and TARGET AML cohorts contain numerous patients),
686 no difference in estimated clonality or monoclonal/polyclonal balance was observed between cohorts
687 (p=0.7 and p=0.65 respectively by Fisher's exact test), and although a trend towards decreased
688 mutational clonality with increasing age among AYA patients was observed, it was not statistically
689 significant (p=0.2). It is important to note that, owing to variable sequencing depths, we do not have the
690 statistical power to reliably detect clones present in less than 5% of the total sample material, though
691 inclusion of variant allele frequencies as low as 0.1% did not change our results or conclusions regarding
692 mutational clonality. Karyotypic clonality was assessed by parsing ISCN karyotypes of all TARGET and
693 TCGA AML patients and using stemline karyotype to identify the most likely ancestral aberrations for
694 patients with abnormal karyotype. Patients with normal karyotype were assigned a karyotypic clonality
695 of 1, as were patients with all metaphases bearing identical aberrations.

696 **Aberrations predicting induction failure.** A logistic model with terms for *NUP98-NSD1* fusions, *FLT3*
697 mutations, interactions between the preceding, and (any one of) *WT1, EZH2,* or *ASXL1* mutation
698 (mutually exclusive) or deletions of the latter (nearly mutually exclusive), or *KMT2A* rearrangements
699 (also mutually exclusive with the preceding) best fit the data for subjects where the first recorded event
700 was either induction failure (1) or any other outcome (0). All possible nested models with the same
701 terms, and all other models arrived at by penalized logistic regression (using an elastic net penalty with
702 the *glmnet* package[60], with any observed recurrent lesion eligible for inclusion as an independent
703 predictor), yielded inferior fits both in terms of classification error and by Akaike information criterion
704 (AIC). We report the marginal p-value for WT1/ASXL1/EZH2 aberrations as predictors of induction
705 failure in the test based on this model fit.

706 **mRNA Sequencing.** Total RNA quality was verified on Agilent Bioanalyzer RNA nanochip or Caliper GX HT
707 RNA LabChip, with samples passing quality control arrayed into a 96-well plate. PolyA+ RNA was purified
708 using the 96-well MultiMACS mRNA isolation kit on the MultiMACS 96 separator (Miltenyi Biotec) from
709 2µg total RNA with on-column DNaseI-treatment as per the manufacturer's instructions. The eluted
710 PolyA+ RNA was ethanol precipitated and resuspended in 10µL of DEPC treated water with 1:20
711 SuperaseIN (Life Technologies). First-stranded cDNA was synthesized from the purified polyA+RNA using
712 the Superscript cDNA Synthesis kit (Life Technologies) and random hexamer primers at a concentration
713 of 5µM along with a final concentration of 1ug/uL Actinomycin D, followed by Ampure XP SPRI beads on
714 a Biomek FX robot (Beckman-Coulter). The second strand cDNA was synthesized following the
715 Superscript cDNA Synthesis protocol by replacing the dTTP with dUTP in dNTP mix, allowing second
716 strand to be digested using UNG (Uracil-N-Glycosylase, Life Technologies, USA) in the post-adapter
717 ligation reaction and thus achieving strand specificity. The cDNA was quantified by PicoGreen (Life
718 Technologies) and VICTOR^{3}V Fluorimeter (PerkinElmer). The cDNA was fragmented by Covaris E210
719 sonication for 55 seconds at a "Duty cycle" of 20% and "Intensity" of 5. The paired-end sequencing
720 library was prepared following the BC Cancer Agency Genome Sciences Centre strand-specific, plate-
721 based and paired-end library construction protocol on a Biomek FX robot (Beckman-Coulter, USA).
722 Briefly, the cDNA was purified in 96-well format using Ampure XP SPRI beads, and was subject to end-
723 repair, and phosphorylation by T4 DNA polymerase, Klenow DNA Polymerase, and T4 polynucleotide
724 kinase respectively in a single reaction, followed by cleanup using Ampure XP SPRI beads and 3' A-tailing
725 by Klenow fragment (3' to 5' exo minus). After purification using Ampure XP SPRI beads, picogreen
726 quantification was performed to determine the amount of Illumina PE adapters to be used in the next
727 step of adapter ligation reaction. The adapter-ligated products were purified using Ampure XP SPRI
728 beads, and digested with UNG (1U/µl) at 37oC for 30 min followed by deactivation at 95oC for 15 min.
729 The digested cDNA was purified using Ampure XP SPRI beads, and then PCR-amplified with Phusion DNA
730 Polymerase (Thermo Fisher) using Illumina's PE primer set, with cycle condition 98˚C 30sec followed by
731 10-13 cycles of 98˚C 10 sec, 65˚C 30 sec and 72˚C 30 sec, and then 72˚C 5min. The PCR products were
732 purified using Ampure XP SPRI beads, and checked with Caliper LabChip GX for DNA samples using the
733 High Sensitivity Assay (PerkinElmer, Inc. USA). PCR product of the desired size range was purified using
734 8% PAGE, and the DNA quality was assessed and quantified using an Agilent DNA 1000 series II assay
735 and Quant-iT dsDNA HS Assay Kit using Qubit fluorometer (Invitrogen), then diluted to 8nM. The final
736 library concentration was double checked and determined by Quant-iT dsDNA HS Assay again for
737 Illumina Sequencing.

738 **mRNA Quantification.** Illumina paired-end RNA sequencing reads were aligned to GRCh37-lite genome-
739 plus-junctions reference using BWA version 0.5.7. This reference combined genomic sequences in the
740 GRCh37-lite assembly and exon-exon junction sequences whose corresponding coordinates were
741 defined based on annotations of any transcripts in Ensembl (v69), Refseq and known genes from the
742 UCSC genome browser, which was downloaded on August 19 2010, August 8 2010, and August 19 2010,
743 respectively. Reads that mapped to junction regions were then repositioned back to the genome, and
744 were marked with 'ZJ:Z' tags. BWA is run using default parameters, except that the option (-s) is included
745 to disable Smith-Waterman alignment. Finally, reads failing the Illumina chastity filter are flagged with a
746 custom script, and duplicated reads were flagged with Picard Tools. Gene, isoform, and exon-level
747 quantification was performed as previously described[61].

748 **Fusion mRNA Transcript Detection.** Transcriptomic data were de novo assembled using ABySS (v1.3.2)
749 and trans-ABySS (v1.4.6)[62]. For RNA-seq assembly alternate k-mers from k50-k96 were performed using
750 positive strand and ambiguous stand reads as well as negative strand and ambiguous strand reads. The
751 positive and negative strand assemblies were extended where possible, merged and then concatenated
752 together to produce a meta-assembly contig dataset. Large scale rearrangements and gene fusions from
753 RNA-seq libraries were identified from contigs that had high confidence GMAP (v2012-12-20) alignments
754 to two distinct genomic regions. Evidence for the alignments were provided from aligning reads back to
755 the contigs and from aligning reads to genomic coordinates. Events were then filtered on read
756 thresholds. Insertions and deletions were identified by gapped alignment of contigs to the human
757 reference using GMAP. The events were then screened against dbSNP and other variation databases to
758 identify putative novel events.

759 **miRNA Sequencing.** Small RNAs, containing microRNA (miRNA), in the flow-through material following
760 mRNA purification on a MultiMACS separator (Miltenyi Biotec) are recovered by ethanol precipitation.
761 miRNA-seq libraries are constructed using a 96-well plate-based protocol developed at the BC Cancer
762 Agency, Genome Sciences Centre. Briefly, an adenylated single-stranded DNA 3' adapter is selectively
763 ligated to miRNAs using a truncated T4 RNA ligase2 (New England Biolabs). An RNA 5' adapter is then
764 added, using a T4 RNA ligase (Ambion) and ATP. Next, first strand cDNA is synthesized using Superscript
765 II Reverse Transcriptase (Invitrogen), and serves as the template for PCR. Index sequences (6
766 nucleotides) are introduced at this PCR step to enable multiplexed pooling of miRNA libraries. PCR
767 products are pooled, then size-selected on an in-house developed 96-channel robot to enrich the miRNA
768 containing fraction and remove adapter contaminants. Each size-selected indexed pool is ethanol
769 precipitated and quality checked on an Agilent Bioanalyzer DNA 1000 chip and quantified using a Qubit
770 fluorometer (Invitrogen, cat. Q32854). Each pool is then diluted to a target concentration for cluster
771 generation and loaded into a single lane of a HiSeq 2000 flow cell for sequencing with a 31-bp main read
772 (for the insert) and a 7-bp read for the index.

773 Sequence data are separated into individual samples based on the index read sequences, and the reads
774 undergo an initial QC assessment. Adapter sequence is then trimmed off, and the trimmed reads for
775 each sample are aligned to the NCBI GRCh37-lite reference genome.

776 Routine QC assesses a subset of raw sequences from each pooled lane for the abundance of reads from
777 each indexed sample in the pool, the proportion of reads that possibly originate from adapter dimers
778 (i.e. a 5' adapter joined to a 3' adapter with no intervening biological sequence) and for the proportion
779 of reads that map to human miRNAs. Sequencing error is estimated by a method originally developed
780 for SAGE.

781 Libraries that pass this QC stage are preprocessed for alignment. While the size-selected miRNAs vary
782 somewhat in length, typically they are ~21 bp long, and so are shorter than the 31-bp read length. Given
783 this, each read sequence extends some distance into the 3' sequencing adapter. Because this non-
784 biological sequence can interfere with aligning the read to the reference genome, 3' adapter sequence is
785 identified and removed (trimmed) from a read. The adapter-trimming algorithm identifies as long an
786 adapter sequence as possible, allowing a number of mismatches that depends on the adapter length
787 found. A typical sequencing run yields several million reads; using only the first (5') 15 bases of the 3'
788 adapter in trimming makes processing efficient, while minimizing the chance that a miRNA read will
789 match the adapter sequence.

790 After each read has been processed, a summary report is generated containing the number of reads at
791 each read length. Any trimmed read that is shorter than 15bp is discarded; remaining reads are
792 submitted for alignment to the reference genome. BWA (Li and Durbin, 2009) alignment(s) for each read
793 are checked with a series of three filters. A read with more than 3 alignments is discarded as too
794 ambiguous. Only perfect alignments with no mismatches are used. Reads that fail the Illumina
795 basecalling chastity filter are retained, while reads that have soft-clipped CIGAR strings are discarded.

796 For reads retained after filtering, each coordinate for each read alignment is annotated using a
797 reference database, and requiring a minimum 3-bp overlap between the alignment and an annotation. If
798 a read has more than one alignment location, and the annotations for these are different, we use a
799 priority list to assign a single annotation to the read, as long as only one alignment is to a miRNA. When
800 there are multiple alignments to different miRNAs, the read is flagged as cross-mapped (de Hoon et al.,
801 2010), and all of its miRNA annotations are preserved, while all of its non-miRNA annotations are
802 discarded. This ensures that all annotation information about ambiguously mapped miRNAs is retained,
803 and allows annotation ambiguity to be addressed in downstream analyses. Note that we consider
804 miRNAs to be cross-mapped only if they map to different miRNAs, not to functionally identical miRNAs
805 that are expressed from different locations in the genome. Such cases are indicated by miRNA miRBase
806 names, which can have up to 4 separate sections separated by "-", e.g. hsa-mir-26a-1. A difference in
807 the final (e.g. '-1') section denotes functionally equivalent miRNAs expressed from different regions of
808 the genome, and we consider only the first 3 sections (e.g. 'hsa-mir-26a') when comparing names. As
809 long as a read maps to multiple miRNAs for which the first 3 sections of the name are identical (e.g. hsa-
810 mir-26a-1 and hsa-mir-26a-2), it is treated as if it maps to only one miRNA, and is not flagged as cross-
811 mapped.

812 The minimum depth of sequencing required to detect the miRNAs that are expressed in one sample is
813 1,000,000 reads per library mapped to miRBase (v21) annotations. Finally, for each sample, the reads
814 that correspond to particular miRNAs are summed and normalized to a million miRNA-aligned reads to
815 generate the quantification files. TARGET and TCGA miRNA quantifications were normalized with pSVA,
816 preserving known subtype-specific miRNA expression patterns, prior to comparison[63].

817 Differentially expressed miRNAs and mRNA were determined by Wilcoxon tests, where significantly
818 differentially expressed miRNAs were those with Benjamini-Hochberg multiple test corrected p-values
819 <0.05. Correlation between miRNA and mRNA expression was determined using the Spearman
820 correlation.

821 **DNA-methylation analysis.** Bisulfite conversion of genomic DNA was performed with EZ DNA
822 methylation Kit (Zymo Research, Irvine, CA) following the manufacturer's protocol with modifications for
823 the Infinium Methylation Assay. Briefly, one microgram of genomic DNA was mixed with 5 µl of Dilution
824 Buffer and incubated at 37°C for 15 minutes and then mixed with 100 µl of conversion reagent prepared
825 as instructed in the protocol. Mixtures were incubated in a thermocycler for 16 cycles at 95°C for 30
826 seconds and 50°C for 60 minutes. Bisulfite-converted DNA samples were loaded onto the provided 96-
827 column plates for desulphonation, washing and elution. The concentration of bisulfite-converted, eluted
828 DNA was measured by UV-absorbance using a NanoDrop-1000 (Thermo Fisher Scientific, Waltham, MA).
829 Bisulfite-converted genomic DNA was analyzed using the Infinium Human Methylation27 Beadchip Kit
830 (Illumina, San Diego, CA, #WG-311-1202). DNA amplification, fragmentation, array hybridization,
831 extension and staining were performed with reagents provided in the kit according to the

832 manufacturer's protocol (Illumina Infinium II Methylation Assay, #WG-901-2701). Briefly, 4 µl of
833 bisulfite-converted genomic DNA at a minimum concentration of 20 ng/µL) was added to 0.8 ml 96-well
834 storage plate (Thermo Fisher Scientific), denatured in 0.014N sodium hydroxide, neutralized and then
835 amplified for 20-24 hours at 37°C. Samples were fragmented at 37°C for 60 minutes and precipitated in
836 isopropanol. Re-suspended samples were denatured in a 96-well plate heat block at 95°C for 20
837 minutes. 15 µl of each sample was loaded onto a 12-sample BeadChip, assembled in the hybridization
838 chamber as instructed by the manufacturer and incubated at 48°C for 16-20 hours. Following
839 hybridization, the BeadChips were washed and assembled in a fluid flow-through station for primer-
840 extension reaction and staining with reagents and buffers provided. Polymer-coated BeadChips were
841 scanned in an iScan scanner (Illumina) using Inf Methylation mode. For both HumanMethylation27 and
842 HumanMethylation450 arrays, methylated and unmethylated signal intensity and detection p-values
843 were extracted after background correction and (in the case of HumanMethylation450 arrays) dye-bias
844 equalization by normal-exponential convolution (noob[64]) as implemented in the minfi package[65]. Data
845 from HumanMethylation450 arrays were additionally normalized using functional normalization
846 (funnorm[66]) as implemented in the minfi package, then summarized as beta values [M /(M+U)]. Probes
847 with an annotated SNV within the CpG or single-base extension site are masked as NA across all
848 samples. Probes with non-detection probability > 0.01 are masked as NA for individual samples.

849 **Transcriptional silencing evaluation and tabulation**

850 Transcription is influenced by a large number of features, among which is methylation of genomic CpG
851 dinucleotides, which often leads to methyl-binding domain proteins excluding transcriptional activators
852 when it occurs near a transcription start site. Not all gene promoters are influenced by differences in
853 DNA methylation, and not all promoters which are thusly influenced are relevant in a given cell type.
854 Thus we sought to identify bundles of transcripts (genes) whose expression appears to be influenced by
855 promoter CpG methylation and whose expression potential is perturbed in a subset of AML cases.

856 To establish a uniform criteria for "calling" such events, we evaluated over 50,000 loci from the Illumina
857 HumanMethylation450 ("450k") microarray near the transcription start sites of over 20,000 transcripts.
858 Where any variance in transcript abundance was explained by variation in DNA methylation levels at a
859 locus, we retained the locus and gene symbol for further evaluation. With this set of several thousand
860 potential marker pairs, we iteratively sought "silencing" cutoff points, such that the maximum
861 expression of a gene in any sample with methylation above the cutoff level was less than or equal to the
862 median expression of samples below the cutoff. The relative levels of DNA methylation and expression
863 appeared to differ systematically between TCGA AML and TARGET AML patients. Therefore we retained
864 the most conservative (highest) cut-point from among the two cohorts. A large number of TARGET AML
865 patients were previously assayed on the promoter-centric Illumina HumanMethylation27 ("27k")
866 microarray; to maximize the sample size for silencing calls, we performed the same conservative
867 procedure as described above with 27k loci. Whenever a locus could be found with a suitable cut-point
868 on both 27k and 450k arrays, we used the two loci to cross-validate transcriptional silencing behavior
869 between the two (largely disjoint) sets of samples (TCGA AML patients were assayed on both 27k and
870 450k arrays, so we used the appropriate complementary assay to cross-validate each cutoff in TCGA).
871 The resulting set of "tag CpGs" (loci with satisfactory cutoff values for a given gene) on each platform,
872 along with the results of applying these cutoffs to dichotomize patient samples into "silenced" or not,
873 are provided in **Table S9**. Selected loci and genes affected across multiple patients are plotted in **Fig. 5a**,
874 annotated within each major cytogenetic group by the fraction of patients silenced.

875 **Non-negative matrix factorization, DNA methylation signature derivation, and hierarchical clustering**

876 Non-negative matrix factorization (NMF) decomposes a strictly positive data matrix *X* (with *N* rows and
877 *M* columns) into a lower-dimensional *N*x*K* weight matrix *W* and a corresponding *K*x*M* score matrix *H*[67].
878 The crux of the decomposition is to find coefficients for *W* and *H* which, when multiplied, most closely
879 recover the original high-dimensional data matrix *X*, as there is no guarantee that a global optimum
880 exists in the absence of further constraints. This can be approached as an optimization problem: given
881 an estimate of the underlying rank *K* for the weight matrix *W*, what coefficients minimize the squared
882 reconstruction error $(X–WH)^2$? When this is formulated as a non-negative least squares fit, alternating
883 between fits for *W* and *H* at each iteration, a fast sequential coordinate descent procedure implemented
884 by Eric Xihui Lin (https://cran.r-project.org/web/packages/NNLM/vignettes/Fast-And-Versatile-
885 NMF.html) is useful for the large matrix we use for the input *X*. To decrease the size of *X* without
886 discarding information, the HumanMethylation450 data was further collapsed by aggregating signals at
887 adjacent CpG sites (up to 50bp separated) using the cpgCollapse function in the minfi package, yielding
888 221,406 discrete clustered methylation measurements, of which approximately half (118,586) showed
889 non-negligible variation across diagnostic tumor samples and/or matched remission samples. The
890 underlying identifiable rank *K* of the low-dimensional weight matrix *W* was estimated by 5-fold cross-
891 validation, using random row x column knockouts (set to NA) in 20% of the matrix entries for each fold,
892 followed by minimization of reconstruction error and maximization of inferred rank. Based on this
893 procedure, the optimal rank *K* (with mean absolute error of 0.02793436) for *W* was estimated as 31. By
894 masking with *W* and *H* matrices derived from normal bone marrow populations (for which *K* was chosen
895 as 13, again based on reconstruction error as above), we subtracted "normal" hematopoietic cell signals
896 and simultaneously estimated the purity (cellularity) of each tumor sample, which allowed us to amplify
897 disease-specific signals, correcting *in silico* for estimated purity on a logit scale, and finally transforming
898 back to the original proportional 0-1 scale for presentation in **Fig. 5b**. The 31-row by 284-column patient
899 score matrix *H,* are provided in **Table S10**; selected signatures of particular interest are plotted in **Fig.**
900 **5b**. Ward's method was employed to cluster columns (patients) in the figure panel by Manhattan
901 distance.

902 **Survival analysis.**

903 We tested an additional cohort of pediatric AML patients for outcome measures associated with
904 alterations of *FLT3*-ITD, *NPM1* and *WT1* mutations and *NUP98-NSD1* translocations (**Fig. 3C**, lower right,
905 and **Fig. S13**, abbreviated "DCOG"). Patient data for this cohort was provided by the Dutch Childhood
906 Oncology group (DCOG), the AML 'Berlin-Frankfurt-Münster' Study Group (AML-BFM-SG), the Czech
907 Pediatric Hematology (CPH) group, the St Louis Hospital in Paris, France, the Medical Research Council
908 (MRC), and the Italian Association for Pediatric Hematology and Oncology (AIEOP). Patients were
909 treated by LAME 86, DCOG/AML-BFM 87, DCOG 92-94/AML-BFM 93, AML-BFM 98, AEIOP-2002/01,
910 ELAM02, AML-BFM 04 and MRC-12/15 protocols[68-75]. These protocols consisted of 4-5 blocks of
911 intensive chemotherapy, using a standard cytarabine and anthracycline backbone. All patients in this
912 cohort were previously published by Balgobind et al.[76], and were extensively screened by RT-PCR or FISH
913 for recurrent aberrations, such as *KMT2A*-rearrangements, *RUNX1-RUNX1T1*, *CBFB-MYH11*, *PML-RARA*,
914 *NUP98*-rearrangements, *FLT3*-ITD, and mutations in *NPM1*, *CEBPA*, *WT1*, *N/KRAS* and *c-KIT*[76-79], and
915 included 326 patients with data available on *NUP98-NSD1*, *NPM1*, *FLT3*-ITD and *WT1* status. Complete
916 remission was obtained in 74.8% of the patients. A total of 114 patients (35.0%) received a HSCT, of

917 which 35 (10.7%) received an HSCT at first complete remission. The median follow up time of survivors
918 was 4.5 years (range 0.3-28 years) and the cohort-wide OS and EFS were 59.5% and 41.9%, respectively.

919 The Kaplan-Meier method was used to estimate overall survival (OS) and event free survival (EFS). OS is
920 defined as the time from study entry until death. EFS is defined as the time from study entry until death,
921 induction failure, or relapse. Patients lost to follow-up were censored at their date of last known
922 contact. Comparisons of OS and EFS were made using the log-rank test.

923 TARGET and TCGA subjects were combined in Cox proportional hazards fits for association of DNA
924 methylation signatures with survival outcome, and model parameters for well-established risk factors
925 (*TP53* mutation, white blood cell count at diagnosis) were also estimated. Due to the nonlinear
926 association of age with survival in pediatric AML patients, and the difficulty of properly evaluating this
927 relationship, we instead stratified the Cox proportional hazards fits by cohort.

928 For miRNA associated survival analyses, the expression (RPM) cut point between high and low
929 expression groups for each miRNA was defined using the X-tile method[80], where all separation points
930 between patients were considered and the selected cut point was the one that provided the optimal
931 (lowest) EFS log rank p-value.

932 **Life Sciences Reporting Summary**

933 For additional information on experimental design, methods and reagents, please see the associated "Life
934 Sciences Reporting Summary Report" file.

935 **Data Availability**

936 Complete details of sample preparation protocols, clinical annotations, and all primary data are available
937 through the TARGET Data Matrix (https://ocg.cancer.gov/programs/target/data-matrix). Sequence data
938 are also accessible through the National Cancer Institute Genomic Data Commons
939 ((https://portal.gdc.cancer.gov/legacy-archive/search/f) or the National Center for Biotechnology
940 Information's dbGaP (https://www.ncbi.nlm.nih.gov/gap) under accession number phs000218.

941

942 **Online Methods References**

943 44. Drmanac, R.*, et al.* Human genome sequencing using unchained base reads on self-assembling
944 DNA nanoarrays. *Science* **327**, 78-81 (2010).
945 45. Zhang, J.*, et al.* Germline Mutations in Predisposition Genes in Pediatric Cancer. *N Engl J Med*
946 **373**, 2336-2346 (2015).
947 46. Li, H.*, et al.* The Sequence Alignment/Map format and SAMtools. *Bioinformatics* **25**, 2078-2079
948 (2009).
949 47. Cingolani, P.*, et al.* A program for annotating and predicting the effects of single nucleotide
950 polymorphisms, SnpEff: SNPs in the genome of Drosophila melanogaster strain w1118; iso-2;
951 iso-3. *Fly (Austin)* **6**, 80-92 (2012).
952 48. Cingolani, P.*, et al.* Using Drosophila melanogaster as a Model for Genotoxic Chemical
953 Mutational Studies with a New Program, SnpSift. *Front Genet* **3**, 35 (2012).
954 49. Saunders, C.T.*, et al.* Strelka: accurate somatic small-variant calling from sequenced tumor-
955 normal sample pairs. *Bioinformatics* **28**, 1811-1817 (2012).

956 50. Ye, K., Schulz, M.H., Long, Q., Apweiler, R. & Ning, Z. Pindel: a pattern growth approach to detect
957 break points of large deletions and medium sized insertions from paired-end short reads.
958 *Bioinformatics* **25**, 2865-2871 (2009).
959 51. Zhou, X.*, et al.* Exploring genomic alteration in pediatric cancer using ProteinPaint. *Nat Genet* **48**,
960 4-6 (2016).
961 52. Lawrence, M.S.*, et al.* Discovery and saturation analysis of cancer genes across 21 tumour types.
962 *Nature* **505**, 495-501 (2014).
963 53. Zhang, Y., Zhou, H., Zhou, J. & Sun, W. Regression Models For Multivariate Count Data. *J Comput*
964 *Graph Stat* **26**, 1-13 (2017).
965 54. Leiserson, M.D., Wu, H.-T., Vandin, F. & Raphael, B.J. CoMEt: a statistical approach to identify
966 combinations of mutually exclusive alterations in cancer. *Genome Biology* **16**, 160 (2015).
967 55. Shannon, P.*, et al.* Cytoscape: a software environment for integrated models of biomolecular
968 interaction networks. *Genome Res* **13**, 2498-2504 (2003).
969 56. van Borkulo, C.D.*, et al.* A new method for constructing networks from binary data. *Sci Rep* **4**,
970 5918 (2014).
971 57. Zeileis, A. & Grothendieck, G. zoo: S3 Infrastructure for Regular and Irregular Time Series. *2005*
972 **14**, 27 (2005).
973 58. Mayakonda, A. & Koeffler, H.P. Maftools: Efficient analysis, visualization and summarization of
974 MAF files from large-scale cohort based cancer studies. Preprint at https://
975 www.biorxiv.org/content/early/2016/05/11/052662.
976 59. Miller, C.A.*, et al.* SciClone: inferring clonal architecture and tracking the spatial and temporal
977 patterns of tumor evolution. *PLoS Comput Biol* **10**, e1003665 (2014).
978 60. Friedman, J.H., Hastie, T. & Tibshirani, R. Regularization Paths for Generalized Linear Models via
979 Coordinate Descent. *2010* **33**, 22 (2010).
980 61. Chun, H.J.*, et al.* Genome-Wide Profiles of Extra-cranial Malignant Rhabdoid Tumors Reveal
981 Heterogeneity and Dysregulated Developmental Pathways. *Cancer Cell* **29**, 394-406 (2016).
982 62. Robertson, G.*, et al.* De novo assembly and analysis of RNA-seq data. *Nat Meth* **7**, 909-912
983 (2010).
984 63. Leek, J.T., Johnson, W.E., Parker, H.S., Jaffe, A.E. & Storey, J.D. The sva package for removing
985 batch effects and other unwanted variation in high-throughput experiments. *Bioinformatics* **28**,
986 882-883 (2012).
987 64. Triche, T.J., Jr., Weisenberger, D.J., Van Den Berg, D., Laird, P.W. & Siegmund, K.D. Low-level
988 processing of Illumina Infinium DNA Methylation BeadArrays. *Nucleic Acids Res* **41**, e90 (2013).
989 65. Aryee, M.J.*, et al.* Minfi: a flexible and comprehensive Bioconductor package for the analysis of
990 Infinium DNA methylation microarrays. *Bioinformatics* **30**, 1363-1369 (2014).
991 66. Fortin, J.P.*, et al.* Functional normalization of 450k methylation array data improves replication
992 in large cancer studies. *Genome Biol* **15**, 503 (2014).
993 67. Lee, D.D. & Seung, H.S. Learning the parts of objects by non-negative matrix factorization.
994 *Nature* **401**, 788-791 (1999).
995 68. Abrahamsson, J.*, et al.* Response-guided induction therapy in pediatric acute myeloid leukemia
996 with excellent remission rate. *J Clin Oncol* **29**, 310-315 (2011).
997 69. Burnett, A.K.*, et al.* Identification of patients with acute myeloblastic leukemia who benefit from
998 the addition of gemtuzumab ozogamicin: results of the MRC AML15 trial. *J Clin Oncol* **29**, 369-
999 377 (2011).
1000 70. Creutzig, U.*, et al.* Less toxicity by optimizing chemotherapy, but not by addition of granulocyte
1001 colony-stimulating factor in children and adolescents with acute myeloid leukemia: results of
1002 AML-BFM 98. *J Clin Oncol* **24**, 4499-4506 (2006).

1003 71. Creutzig, U.*, et al.* Treatment strategies and long-term results in paediatric patients treated in
1004 four consecutive AML-BFM trials. *Leukemia* **19**, 2030-2042 (2005).
1005 72. Gibson, B.E.*, et al.* Treatment strategy and long-term results in paediatric patients treated in
1006 consecutive UK AML trials. *Leukemia* **19**, 2130-2138 (2005).
1007 73. Kardos, G.*, et al.* Treatment strategy and results in children treated on three Dutch Childhood
1008 Oncology Group acute myeloid leukemia trials. *Leukemia* **19**, 2063-2071 (2005).
1009 74. Perel, Y.*, et al.* Impact of addition of maintenance therapy to intensive induction and
1010 consolidation chemotherapy for childhood acute myeloblastic leukemia: results of a prospective
1011 randomized trial, LAME 89/91. Leucamie Aique Myeloide Enfant. *J Clin Oncol* **20**, 2774-2782
1012 (2002).
1013 75. Pession, A.*, et al.* Results of the AIEOP AML 2002/01 multicenter prospective trial for the
1014 treatment of children with acute myeloid leukemia. *Blood* **122**, 170-178 (2013).
1015 76. Balgobind, B.V.*, et al.* Integrative analysis of type-I and type-II aberrations underscores the
1016 genetic heterogeneity of pediatric acute myeloid leukemia. *Haematologica* **96**, 1478-1487
1017 (2011).
1018 77. Hollink, I.H.*, et al.* NUP98/NSD1 characterizes a novel poor prognostic group in acute myeloid
1019 leukemia with a distinct HOX gene expression pattern. *Blood* **118**, 3645-3656 (2011).
1020 78. Hollink, I.H.*, et al.* Clinical relevance of Wilms tumor 1 gene mutations in childhood acute
1021 myeloid leukemia. *Blood* **113**, 5951-5960 (2009).
1022 79. Hollink, I.H.*, et al.* Favorable prognostic impact of NPM1 gene mutations in childhood acute
1023 myeloid leukemia, with emphasis on cytogenetically normal AML. *Leukemia* **23**, 262-270 (2009).
1024 80. Camp, R.L., Dolled-Filhart, M. & Rimm, D.L. X-tile: a new bio-informatics tool for biomarker
1025 assessment and outcome-based cut-point optimization. *Clin Cancer Res* **10**, 7252-7259 (2004).

1026

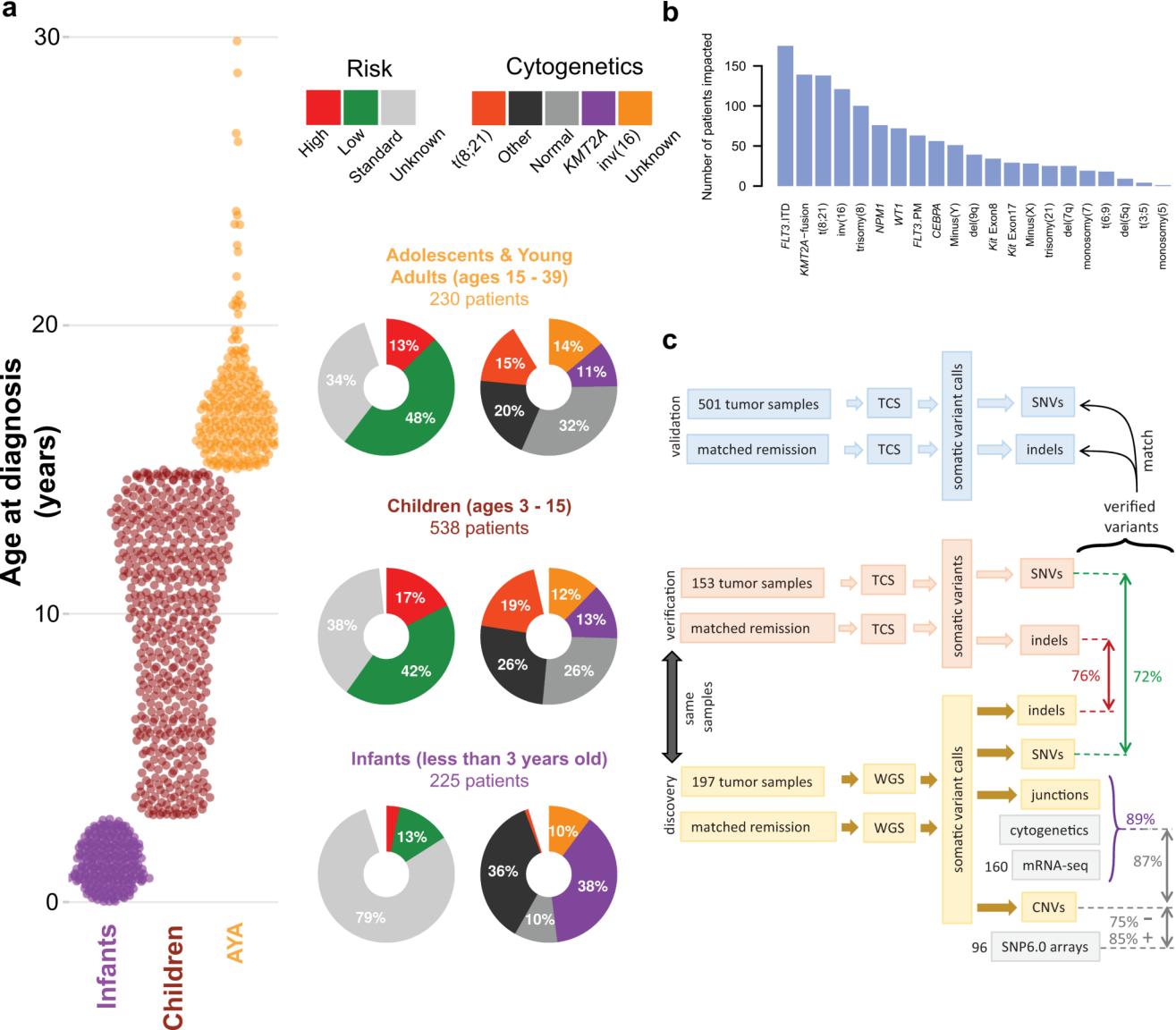
a
Age at diagnosis (years)
30
20
10
0
Infants
Children
AYA
Risk
High
Low
Standard
Unknown
Cytogenetics
t(8;21)
Other
Normal
KMT2A
inv(16)
Unknown
Adolescents & Young Adults (ages 15 - 39)
230 patients
13%
48%
34%
14%
11%
32%
20%
15%
Children (ages 3 - 15)
538 patients
17%
42%
38%
12%
13%
26%
26%
19%
Infants (less than 3 years old)
225 patients
13%
79%
10%
38%
10%
36%
b
Number of patients impacted
150
100
50
0
FLT3.ITD
KMT2A-fusion
t(8;21)
inv(16)
trisomy(8)
NPM1
WT1
FLT3.PM
CEBPA
Minus(Y)
del(9q)
Kit Exon8
Kit Exon17
Minus(X)
trisomy(21)
del(7q)
monosomy(7)
t(6;9)
del(5q)
t(3;5)
monosomy(5)
c
validation
501 tumor samples
matched remission
TCS
TCS
somatic variant calls
SNVs
indels
match
verified variants
verification
153 tumor samples
matched remission
TCS
TCS
somatic variants
SNVs
indels
76%
72%
same samples
discovery
197 tumor samples
matched remission
WGS
WGS
somatic variant calls
indels
SNVs
junctions
cytogenetics
160 mRNA-seq
89%
87%
CNVs
75% −
85% +
96 SNP6.0 arrays

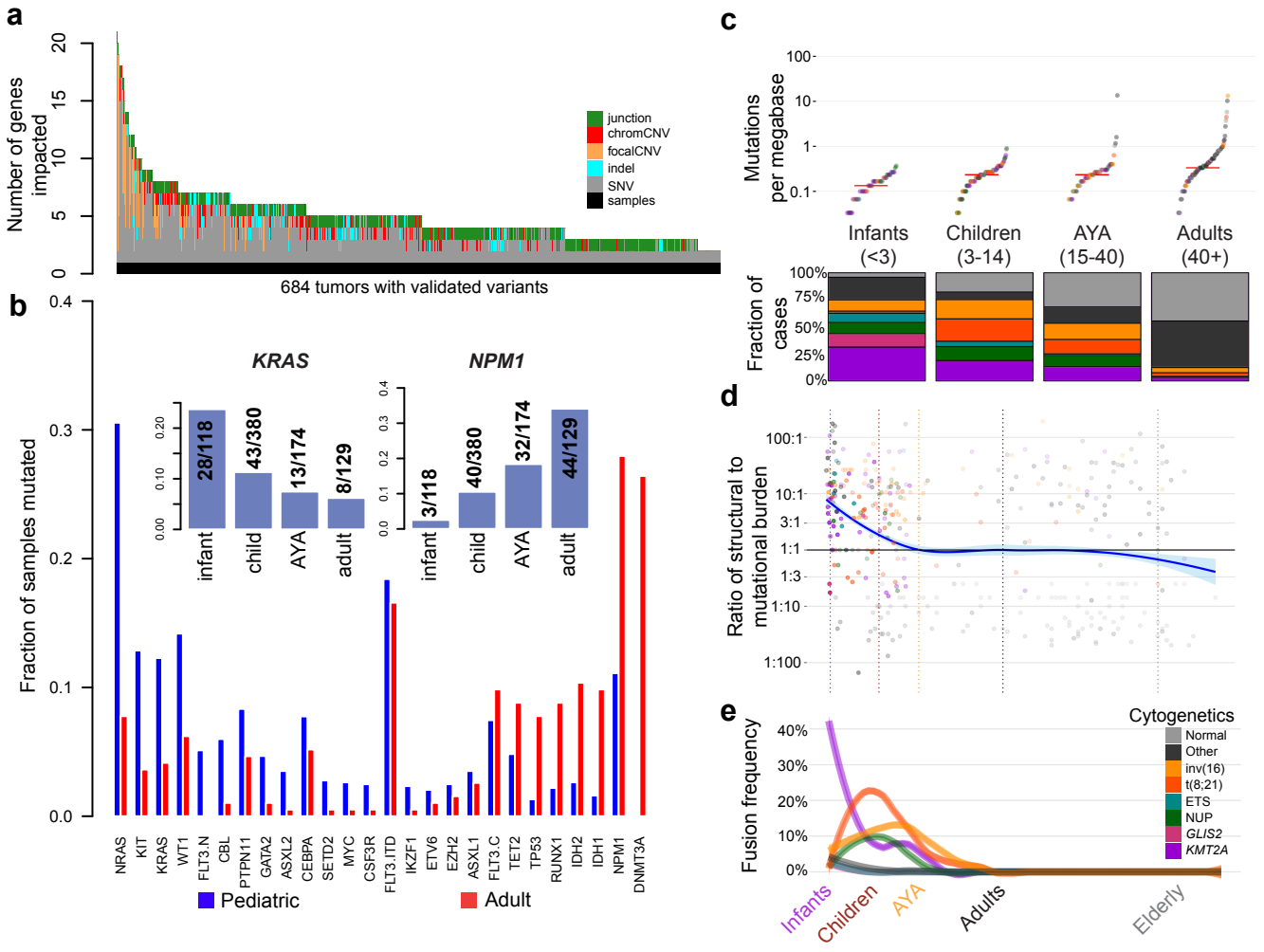
a
Number of genes impacted
0
5
10
15
20
junction
chromCNV
focalCNV
indel
SNV
samples
684 tumors with validated variants
b
Fraction of samples mutated
0.0
0.1
0.2
0.3
0.4
KRAS
NPM1
28/118
43/380
13/174
8/129
3/118
40/380
32/174
44/129
infant
child
AYA
adult
NRAS
KIT
KRAS
WT1
FLT3.N
CBL
PTPN11
GATA2
ASXL2
CEBPA
SETD2
MYC
CSF3R
FLT3.ITD
IKZF1
ETV6
EZH2
ASXL1
FLT3.C
TET2
TP53
RUNX1
IDH2
IDH1
NPM1
DNMT3A
Pediatric
Adult
c
Mutations per megabase
100
10
1
0.1
Infants (<3)
Children (3-14)
AYA (15-40)
Adults (40+)
Fraction of cases
100%
75%
50%
25%
0%
d
Ratio of structural to mutational burden
100:1
10:1
3:1
1:1
1:3
1:10
1:100
e
Fusion frequency
40%
30%
20%
10%
0%
Cytogenetics
Normal
Other
inv(16)
t(8;21)
ETS
NUP
GLIS2
KMT2A
Infants
Children
AYA
Adults
Elderly

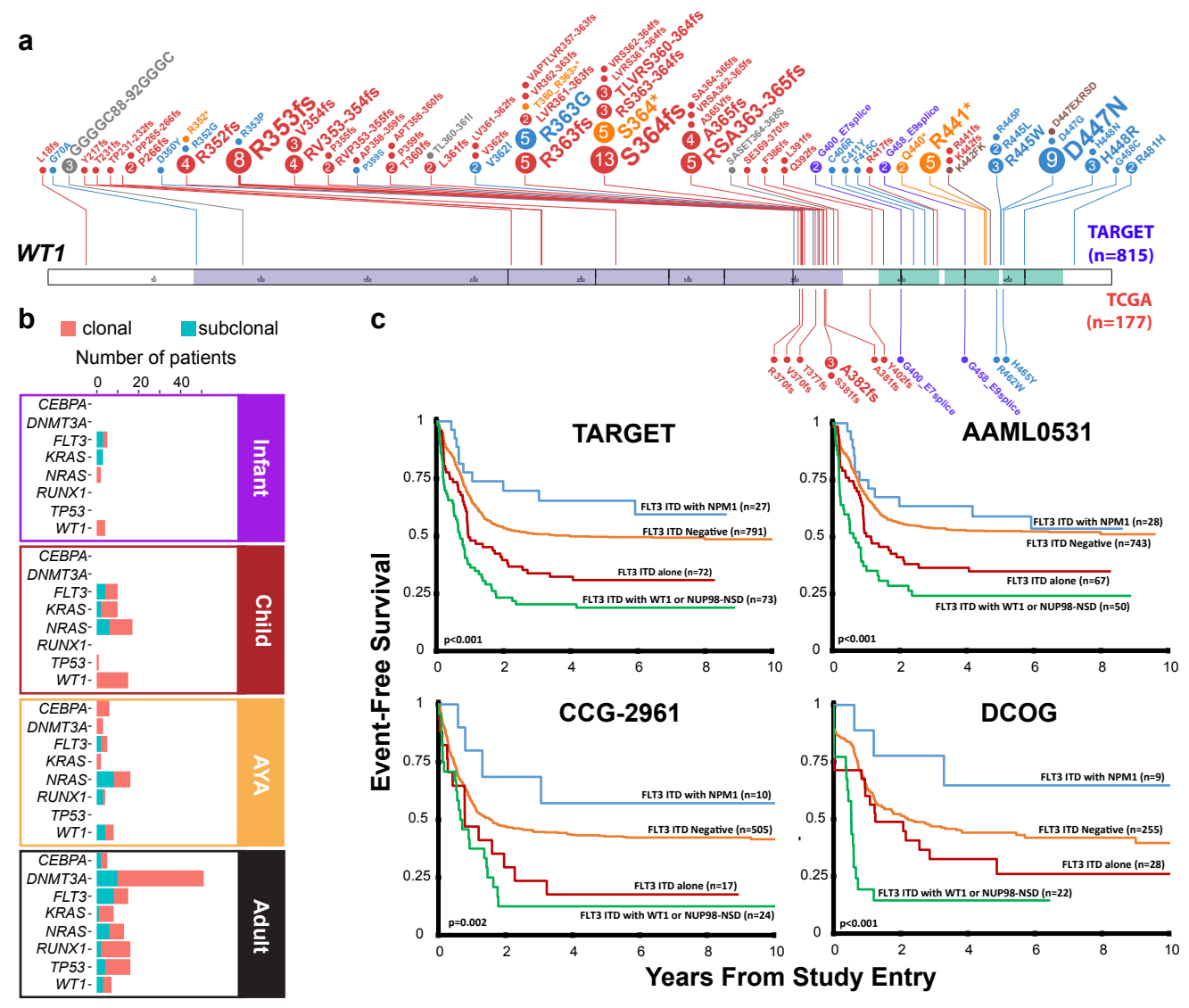
a
WT1
TARGET
(n=815)
TCGA
(n=177)
b
clonal
subclonal
Number of patients
0
20
40
CEBPA-
DNMT3A-
FLT3-
KRAS-
NRAS-
RUNX1-
TP53-
WT1-
Infant
Child
AYA
Adult
c
TARGET
AAML0531
CCG-2961
DCOG
Event-Free Survival
Years From Study Entry
FLT3 ITD with NPM1 (n=27)
FLT3 ITD Negative (n=791)
FLT3 ITD alone (n=72)
FLT3 ITD with WT1 or NUP98-NSD (n=73)
p<0.001
FLT3 ITD with NPM1 (n=28)
FLT3 ITD Negative (n=743)
FLT3 ITD alone (n=67)
FLT3 ITD with WT1 or NUP98-NSD (n=50)
p<0.001
FLT3 ITD with NPM1 (n=10)
FLT3 ITD Negative (n=505)
FLT3 ITD alone (n=17)
FLT3 ITD with WT1 or NUP98-NSD (n=24)
p=0.002
FLT3 ITD with NPM1 (n=9)
FLT3 ITD Negative (n=255)
FLT3 ITD alone (n=28)
FLT3 ITD with WT1 or NUP98-NSD (n=22)
p<0.001

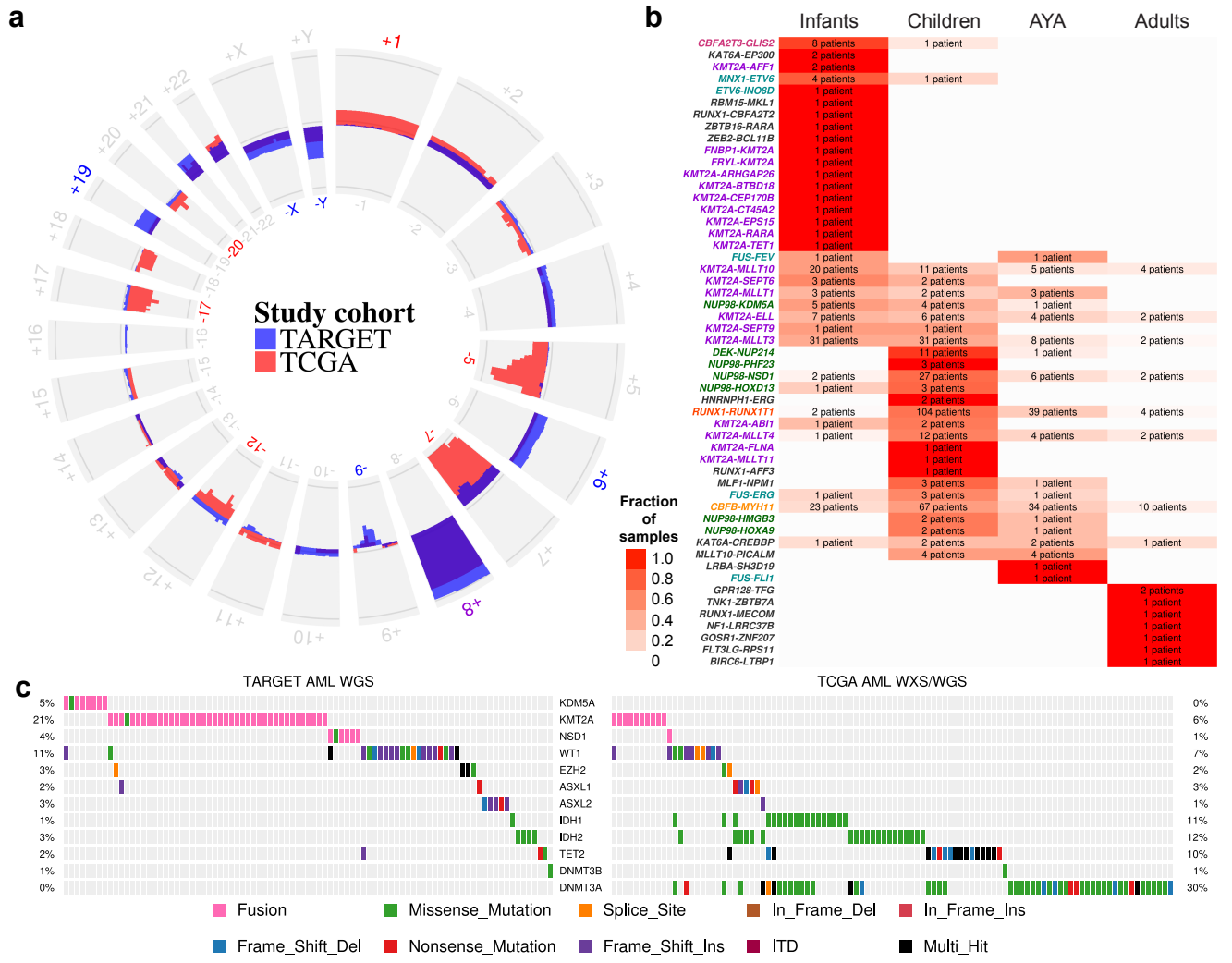
a
Study cohort
TARGET
TCGA
Fraction of samples
1.0
0.8
0.6
0.4
0.2
0
b
Infants
Children
AYA
Adults
CBFA2T3-GLIS2
KAT6A-EP300
KMT2A-AFF1
MNX1-ETV6
ETV6-INO8D
RBM15-MKL1
RUNX1-CBFA2T2
ZBTB16-RARA
ZEB2-BCL11B
FNBP1-KMT2A
FRYL-KMT2A
KMT2A-ARHGAP26
KMT2A-BTBD18
KMT2A-CEP170B
KMT2A-CT45A2
KMT2A-EPS15
KMT2A-RARA
KMT2A-TET1
FUS-FEV
KMT2A-MLLT10
KMT2A-SEPT6
KMT2A-MLLT1
NUP98-KDM5A
KMT2A-ELL
KMT2A-SEPT9
KMT2A-MLLT3
DEK-NUP214
NUP98-PHF23
NUP98-NSD1
NUP98-HOXD13
HNRNPH1-ERG
RUNX1-RUNX1T1
KMT2A-ABI1
KMT2A-MLLT4
KMT2A-FLNA
KMT2A-MLLT11
RUNX1-AFF3
MLF1-NPM1
FUS-ERG
CBFB-MYH11
NUP98-HMGB3
NUP98-HOXA9
KAT6A-CREBBP
MLLT10-PICALM
LRBA-SH3D19
FUS-FLI1
GPR128-TFG
TNK1-ZBTB7A
RUNX1-MECOM
NF1-LRRC37B
GOSR1-ZNF207
FLT3LG-RPS11
BIRC6-LTBP1
8 patients
2 patients
2 patients
4 patients
1 patient
1 patient
1 patient
1 patient
1 patient
1 patient
1 patient
1 patient
1 patient
1 patient
1 patient
1 patient
1 patient
20 patients
3 patients
3 patients
5 patients
7 patients
1 patient
31 patients
2 patients
1 patient
2 patients
1 patient
2 patients
104 patients
1 patient
1 patient
1 patient
1 patient
1 patient
1 patient
3 patients
1 patient
23 patients
2 patients
1 patient
4 patients
1 patient
1 patient
1 patient
1 patient
1 patient
1 patient
1 patient
1 patient
1 patient
1 patient
1 patient
1 patient
1 patient

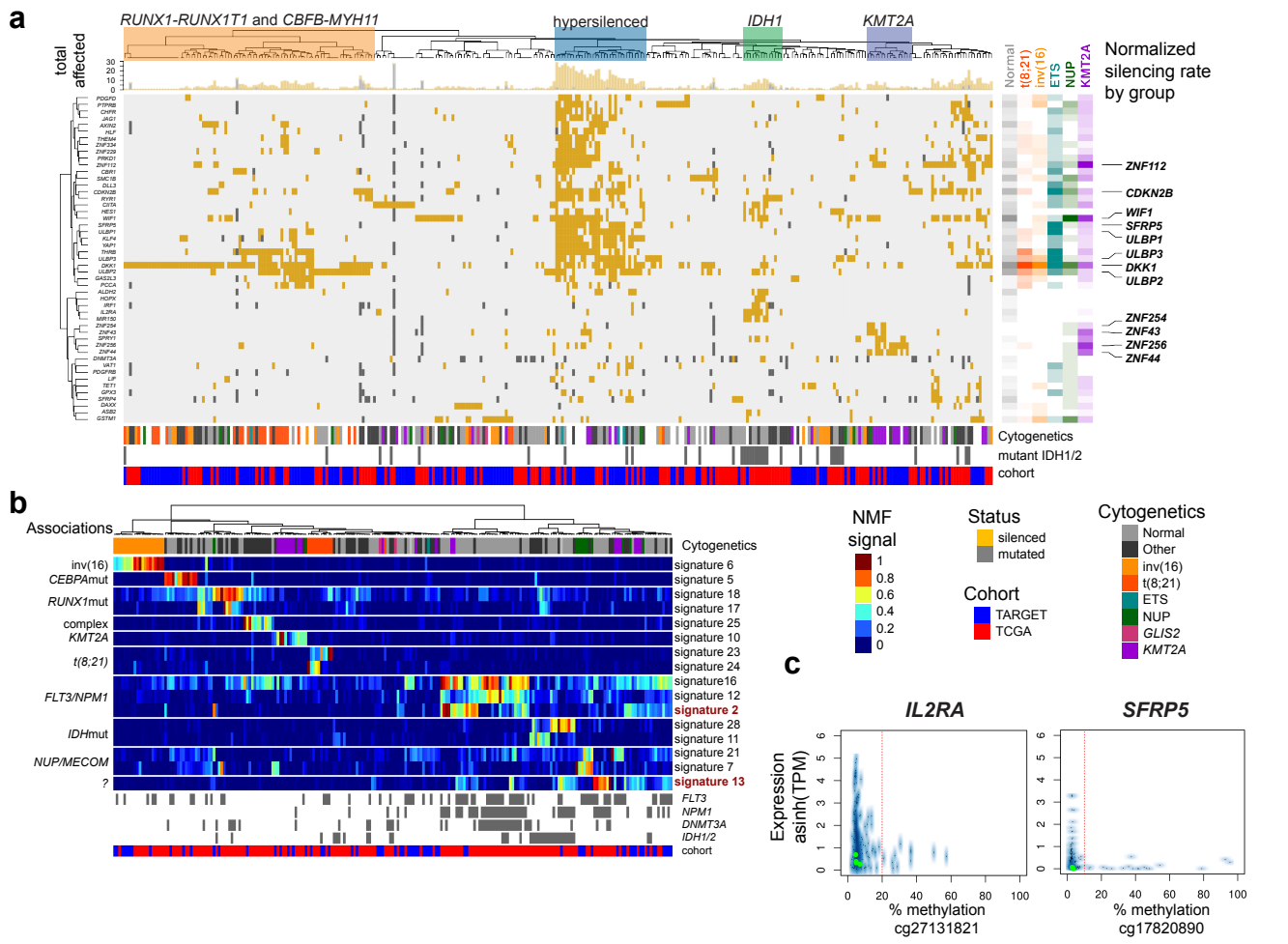
a
RUNX1-RUNX1T1 and CBFB-MYH11
hypersilenced
IDH1
KMT2A
total affected
Normal
t(8;21)
inv(16)
ETS
NUP
KMT2A
Normalized silencing rate by group
ZNF112
CDKN2B
WIF1
SFRP5
ULBP1
ULBP3
DKK1
ULBP2
ZNF254
ZNF43
ZNF256
ZNF44
Cytogenetics
mutant IDH1/2
cohort
b
Associations
Cytogenetics
inv(16)
CEBPAmut
RUNX1mut
complex
KMT2A
t(8;21)
FLT3/NPM1
IDHmut
NUP/MECOM
?
signature 6
signature 5
signature 18
signature 17
signature 25
signature 10
signature 23
signature 24
signature16
signature 12
signature 2
signature 28
signature 11
signature 21
signature 7
signature 13
FLT3
NPM1
DNMT3A
IDH1/2
cohort
NMF signal
1
0.8
0.6
0.4
0.2
0
Status
silenced
mutated
Cohort
TARGET
TCGA
Cytogenetics
Normal
Other
inv(16)
t(8;21)
ETS
NUP
GLIS2
KMT2A
c
IL2RA
SFRP5
Expression asinh(TPM)
% methylation
cg27131821
% methylation
cg17820890

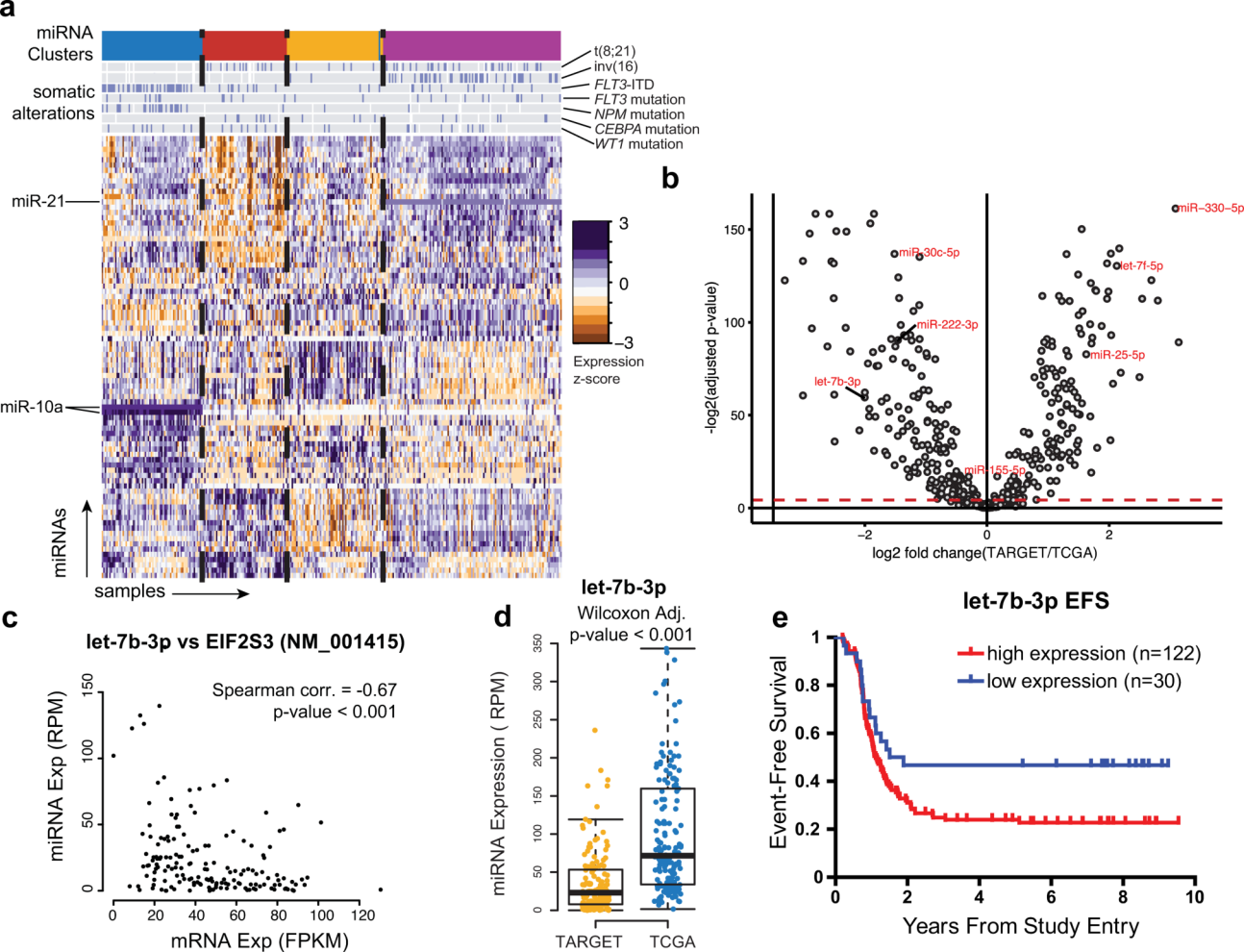
a
miRNA Clusters
somatic alterations
t(8;21)
inv(16)
FLT3-ITD
FLT3 mutation
NPM mutation
CEBPA mutation
WT1 mutation
miR-21
miR-10a
miRNAs
samples
3
0
−3
Expression z-score
b
miR−330−5p
miR-30c-5p
let-7f-5p
miR-222-3p
miR-25-5p
let-7b-3p
miR-155-5p
-log2(adjusted p-value)
log2 fold change(TARGET/TCGA)
c
let-7b-3p vs EIF2S3 (NM_001415)
Spearman corr. = -0.67
p-value < 0.001
miRNA Exp (RPM)
mRNA Exp (FPKM)
d
let-7b-3p
Wilcoxon Adj. p-value < 0.001
miRNA Expression (RPM)
TARGET
TCGA
e
let-7b-3p EFS
high expression (n=122)
low expression (n=30)
Event-Free Survival
Years From Study Entry